12.70 (12.96). Complexes **5c** $Fe(TTP)(C_8H_{10}O_2)_2 \cdot 2H_2O$: Anal. Calcd (found) for $C_{64}H_{60}N_4FeO_6$: 74.12 (74.92); H, 5.83 (5.70); N, 5.40 (5.51).

Acknowledgment. We thank Dr. A. Gouyette (Institut Gustave Roussy, Villejuif, France) for the mass spectrometry measurements.

Supplementary Material Available: Concerning the X-ray structure of complex **5a**: Table V, thermal parameters for nonhydrogen atoms; Table VI, positional parameters for hydrogen atoms; Table VIII, bond distances; Table IX, bond angles; Table X, least-squares mean planes of interest (13 pages); Table VII, calculated and observed structure factor amplitudes (×10) for all observed reflections (14 pages). Ordering information is given on any current masthead page.

A New Inorganic Ring System: Planar $Fe_3(\mu_2\text{-}SR)_3$ in $[Fe_3(SR)_3X_6]^{3-}$—Synthesis, Structures, and Solution Conformation and Equilibrium

M. A. Whitener,[1a] J. K. Bashkin,[1a,b] K. S. Hagen,[1a] J.-J. Girerd,[1c] E. Gamp,[1d] N. Edelstein,[1d] and R. H. Holm*[1a]

Contribution from the Department of Chemistry, Harvard University, Cambridge, Massachusetts 02138, the Laboratoire de Spectrochimie des Éléments de Transition, ERA CNRS 672, Université de Paris-Sud, F-91405 Orsay, France, and the Materials and Molecular Research Division, Lawrence Berkeley Laboratory, Berkeley, California 94720.
Received December 2, 1985

Abstract: Anaerobic reaction of equimolar FeX_2 and RS^- in acetonitrile affords the trinuclear complexes $[Fe_3(SR)_3X_6]^{3-}$ (with X = Cl and R = Ph (**4a**), *p*-tolyl (**4b**), 2,6-$Me_2C_6H_3$ (**4d**), and X = Br, R = Ph (**4c**)) isolated as Et_4N^+ salts. These species constitute the fourth known type of discrete Fe(II) thiolates, the others being $[Fe(SR)_4]^{2-}$, $[Fe_2(SR)_6]^{2-}$, and $[Fe_4(SR)_{10}]^{2-}$. The following crystallographic results were obtained (crystal system; space group; cell parameters; *Z*; unique data ($I > 3\sigma(I)$); *R* (%)). $(Et_4N)_3$ (**4a**): monoclinic; $C2/c$; a = 24.500 (6) Å, b = 13.488 (3) Å, c = 18.217 (5) Å, β = 110.68 (2)°; 4; 2679; 4.9. $(Et_4N)_3$ (**4d**)·3MeCN: monoclinic: $P2_1/n$; a = 15.07 (1) Å, b = 22.38 (3) Å, c = 20.46 (3) Å, β = 91.5 (1)°; 4, 3311; 9.7. $(Et_4N)_3$ (**4c**)·MeCN: hexagonal, $P\bar{6}2c$; $a = b$ = 13.970 (4) Å, c = 18.274 (3) Å; 2; 890; 5.7. The reaction system $FeBr_2$ + $NaSCH_2Ph$ in acetonitrile yields a different type of compound with the composition $(Et_4N)_2[Fe_4(SCH_2Ph)_6Br_4]$ (**5**): triclinic; $P\bar{1}$; a = 12.874 (2) Å, b = 13.949 (3) Å, c = 43.272 (8) Å, α = 94.85 (2)°, β = 94.07 (2)°, γ = 114.98 (1)°; 4; 7402; 6.7. Anions of type **4** contain a new type of inorganic ring system, $Fe_3(\mu_2\text{-}SR)_3$, distinguished by its nearly or exactly planar conformation and unusually large Fe-S-Fe angles of ~140°, the largest values observed for this angle type. The phenyl groups in **4a** and **4c** (which has imposed C_{3h} symmetry) are coplanar with the Fe_3S_3 rings. In **4d** these groups are rotated by ~90° owing to the steric effects of the methyl groups. Distorted tetrahedral coordination at each Fe(II) atom is completed by two halide ligands. The planar structure is to be contrasted with the chair-type conformation of the rings in **5** and other species with adamantane-like stereochemistry. Ring conformations influence the extent of antiferromagnetic interactions in the solid state. Magnetic susceptibility data of planar **4a** are fit well by two $-J$ values at 19-22 cm^{-1}. For $[Fe_4(SR)_{10}]^{2-}$, containing adamantane-like $Fe_4(\mu_2\text{-}SR)_6$ cages with $Fe_3(\mu_2\text{-}SR)_3$ rings in the chair conformation, best fits of the magnetic data give one $-J$ value at 32 or 36 cm^{-1} and one or two others at 42-66 cm^{-1} depending on the coupling symmetry. MO calculations at the extended Hückel level on $[Fe_3(SH)_3Cl_6]^{3-}$ suggest that the inherently stable conformation of the ring is planar. This structure is set in large measure by the stereochemical preference of the S-Fe-S angle and by transannular nonbonded repulsions. The decrease in Cl···Cl distances from 6.6 to 3.9 Å in changing from the planar to the chair conformation emphasizes the latter effect. In acetonitrile the equilibrium $2[Fe_3(SR)_3X_6]^{3-} \rightleftharpoons [Fe_4(SR)_6X_4]^{2-} + 2[FeCl_4]^{2-}$ has been approached in both directions and is shifted to the left with decreasing temperature. At ≲240 K the formation of $[Fe_3(SR)_3X_6]^{3-}$ is essentially complete. In this temperature range the magnetic moment per Fe atom (μ_{Fe}) is 4.1-4.2 μ_B for **4a** in solution and as its crystalline Et_4N^+ salt. This excellent agreement establishes a planar ring conformation in solution. Thus the results of three crystal structures, MO calculations, and solution and solid state magnetic measurements collectively demonstrate that the near or exact planarity of the Fe_3S_3 cycles in $[Fe_3(SR)_3X_6]^{3-}$ is an intrinsic property.

Previous investigations in this laboratory have demonstrated reactions 1-4 in Figure 1, affording the complexes $[Fe(SR)_4]^{2-}$ (**1**), $[Fe_2(SR)_6]^{2-}$ (**2**), $[Fe_4(SR)_{10}]^{2-}$ (**3**), and $[Fe_3(SR)_3Cl_6]^{3-}$ (**4**).[2-7] Several additional examples of **2** have been prepared by others.[8] The set **1-4**, containing species of varying nuclearity based on tetrahedral Fe(II) coordination, has a number of significant aspects. In reactions with elemental sulfur, **1-3** are precursors to a variety of Fe-S-SR clusters.[2,4,5,9] These same complexes serve as structural prototypes of related thiolate complexes formed by M(II) ions with tetrahedral stereochemical preference. An expanding number of such complexes have been prepared and structurally characterized.[10,11] Complex **4a** (R =

(1) (a) Harvard University. (b) NIH Postdoctoral Fellow, 1984-1985. (c) University of Paris. (d) Lawrence Berkeley Laboratory.
(2) Hagen, K. S.; Reynolds, J. G.; Holm, R. H. *J. Am. Chem. Soc.* **1981**, *103*, 4054.
(3) Hagen, K. S.; Stephan, D. W.; Holm, R. H. *Inorg. Chem.* **1982**, *21*, 3928.
(4) Hagen, K. S.; Holm, R. H. *J. Am. Chem. Soc.* **1982**, *104*, 5496.
(5) Hagen, K. S.; Watson, A. D.; Holm, R. H. *J. Am. Chem. Soc.* **1983**, *105*, 3905.
(6) Hagen, K. S.; Holm, R. H. *Inorg. Chem.* **1984**, *23*, 418.
(7) Holm, R. H.; Hagen, K. S., Watson, A. D. In *Chemistry for the Future*; Grünewald, H., Ed.; New York: Pergamon Press, 1984; pp 115-124.
(8) Henkel, G.; Tremel, W.; Krebs, B. *Angew. Chem., Int. Ed. Engl.* **1983**, *22*, 319.
(9) Kurtz, D. M., Jr.; Stevens, W. C. *J. Am. Chem. Soc.* **1984**, *106*, 1523.

0002-7863/86/1508-5607$01.50/0

Table I. Summary of Crystal Data, Intensity Collections, and Structure Refinement Parameters for $(Et_4N)_3[Fe_3(SPh)_3Cl_6]$ (**4a**), $(Et_4N)_3[Fe_3(S\text{-}2,6\text{-}Me_2C_6H_3)_3Cl_6]\cdot 3MeCN$ (**4d**), $(Et_4N)_3[Fe_3(SPh)_3Br_6]\cdot MeCN$ (**4c**), and $(Et_4N)_2[Fe_4(SCH_2Ph)_6Br_4]$ (**5**)

	4a	4d	4c	5
formula	$C_{42}H_{75}Cl_6Fe_3N_3S_3$	$C_{54}H_{96}Cl_6Fe_3N_6S_3$	$C_{44}H_{78}Br_6Fe_3N_4S_3$	$C_{58}H_{82}Br_4Fe_4N_2S_6$
mol wt	1098.53	1305.85	1406.29	1542.70
a, Å	24.500 (6)	15.07 (1)	13.970 (4)	12.874 (2)
b, Å	13.488 (3)	22.38 (3)		13.949 (3)
c, Å	18.217 (5)	20.46 (3)	18.274 (3)	43.272 (8)
α				94.85 (2)
β	110.68 (2)	91.5 (1)		94.07 (2)
γ				114.98 (1)
crystal system	monoclinic	monoclinic	hexagonal	triclinic
V, Å^3	5632 (5)	6896 (15)	3088 (1)	6970 (2)
Z	4	4	2	4
d_{calcd} (d_{obsd}), g/cm^3	1.29 (1.29)	1.26[b]	1.50 (1.51)	1.47 (1.44)
space group	$C2/c$	$P2_1/n$	$P\bar{6}2c$	$P\bar{1}$
cryst size, mm	0.20 × 0.36 × 0.40	0.30 × 0.30 × 0.70	0.65 × 0.45 × 0.45	0.50 × 0.47 × 0.35
radiation (λ, Å)	←	Mo Kᾱ (0.71069)	→	Cu Kᾱ (1.5418)
abs coeff, μ, cm^{-1}	11.9	9.8	46.7	115.5
trans factors (max/min)	0.587/0.560	0.497/0.380	0.042/0.036	0.618/0.002
scan speed, deg/min	2.9–29.3	4.0–29.3	4.0–29.3	2.0–30.0
scan range, deg	2.2	1.0	2.0	1.2
bkgd/scan time ratio	0.25	1.00	1.00	0.25
data collected	$+h,+k,\pm l$	$+h,+k,\pm l$	$+h,+k,+l$	$+h,\pm k,\pm l$
	($3.0 \le 2\theta \le 43°$)	($5.0 \le \omega \le 43.5°$)	($3.0 \le 2\theta \le 60°$)	($4.0 \le 2\theta \le 80°$)
total reflections	5149	9742	3382	11,967
unique data ($I > 3\sigma(I)$)	2679	3311	890	7402
no. of variables	299	365	105	855
$R(R_w)$,[a] %	4.9 (5.3)[d]	9.7 (11.0)[c]	5.7 (8.2)[c]	6.7 (10.3)[c]

[a] $R = \sum||F_o| - |F_c||/\sum|F_o|$; $R_w = [\sum w(|F_o|^2 - |F_c|^2)/\sum w|F_o|^2]^{1/2}$. [b] Accurate density could not be obtained owing to the presence of solvate molecules. [c] Weighting scheme for least-squares refinement: Carruthers, J. R.; Watkin, D. J. *Acta Crystallogr.* **1979**, *A35*, 698. [d] Weighting scheme: $w = [\sigma^2(F) + gF^2]^{-1}$, $g = 0.0009$.

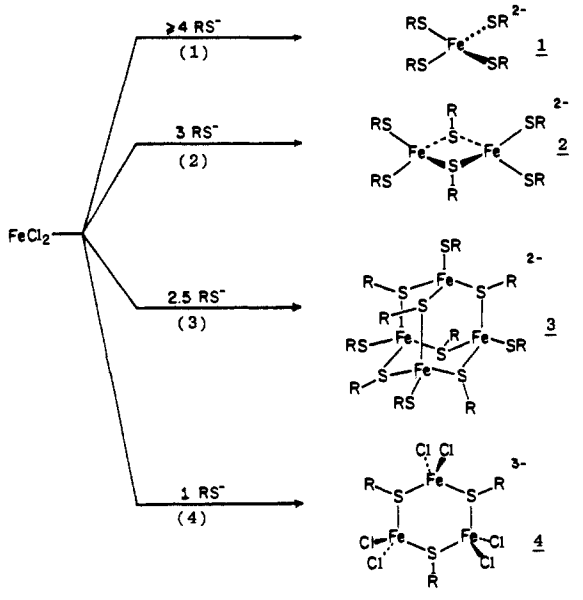

Figure 1. Preparations and schematic structures of the known types of Fe(II) thiolate complexes **1–4**.

Ph), briefly described by us earlier,[4] is one of the few molecules known to contain a $M_3(\mu_2\text{-}SR)_3$ ring. Unlike previous examples,[12-18] whose discrete rings exist in decidedly nonplanar conformations with (usually) unexceptional bond angles, $[Fe_3(SPh)_3Cl_6]^{3-}$ contains a *planar* central ring, phenyl groups that are copolanar with this ring, and remarkably large Fe–S–Fe angles of ~140°.

Our studies of the structures and reactions of complex types **1–3** being largely complete,[2-6] we have turned attention to the cyclic trimers **4**. In terms of the smallest RS^-:Fe(II) ratio, these are the terminal members of the set **1–4**. Reported here are the syntheses, structures, and spectroscopic and magnetic properties and an examination of the conformational stability of this most unusual ring system, as it is found in several type **4** complexes.

Experimental Section

Preparation of Compounds. $(Et_4N)_2[Fe(SEt)_4]$,[5] $(Me_4N)_2[Fe_4(SEt)_{10}]$,[2] and $(n\text{-}Bu_4N)_2[Fe_4(S\text{-}p\text{-}C_6H_4Me)_{10}]$[6] were obtained by published methods. In the following preparations all operations were performed under a pure dinitrogen atmosphere.

$(Et_4N)_3[Fe_3(SPh)_3Cl_6]$ (4a). A solution of 4.78 g (20 mmol) of $(Et_4N)(SPh)$[19] in 60 mL of acetonitrile was added slowly to a stirred solution of 2.52 g (20 mmol) of anhydrous $FeCl_2$ in 50 mL of acetonitrile. A microcrystalline solid began to separate toward the end of the addition. The reaction mixture was cooled to −25 °C. The solid was collected by filtration, washed with 1:3 acetonitrile/ether (v/v), and dried in vacuo to give 5.6 g (77%) of product. This material was recrystallized from 60 mL of acetonitrile, affording 2.8 g (28%) of yellowish-green crystals. Anal. Calcd for $C_{42}H_{75}Cl_6Fe_3N_3S_3$: C, 45.92; H, 6.88; Cl, 19.36; Fe, 15.25; N, 3.83; S, 8.76. Found: C, 45.42; H, 6.86; Cl, 20.14; Fe, 15.03;

(10) $[M_2(SR)_6]^{2-}$—(a) M = Co(II): Reference 6. Tremel, W.; Krebs, B.; Henkel, G. *Angew. Chem., Int. Ed. Engl.* **1984**, *23*, 634. (b) M = Mn(II), Zn(II), Cd(II): Watson, A. D.; Pulla Rao, Ch.; Dorfman, J. R.; Holm, R. H. *Inorg. Chem.* **1985**, *24*, 2820.

(11) $[M_4(SR)_{10}]^{2-}$—(a) M = Mn(II): Costa, T.; Dorfman, J. R.; Hagen, K. S.; Holm, R. H. *Inorg. Chem.* **1983**, *22*, 4091. (b) M = Co(II): Dance, I. G. *J. Am. Chem. Soc.* **1979**, *101*, 6264. (c) M = Zn(II): Hencher, J. L.; Khan, M.; Said, F. F.; Tuck, D. G. *Inorg. Nucl. Chem. Lett.* **1981**, *17*, 287; *Polyhedron* **1985**, *4*, 1263. (d) M = Cd(II): Hagen, K. S.; Holm, R. H. *Inorg. Chem.* **1983**, *22*, 3171.

(12) $Pd_3[S(CH_2CH_2S)_2]_3$: McPartlin, E. M.; Stephenson, N. C. *Acta Crystallogr.* **1969**, *B25*, 1659.

(13) $Pd_3(\mu_2\text{-}SEt)_3(S_2CSEt)_3$: Fackler, J. P., Jr.; Zegarski, W. J. *J. Am. Chem. Soc.* **1973**, *95*, 8566.

(14) $B_3(\mu_2\text{-}SMe)_3X_6$ (X = Cl, Br): Pollitz, S.; Zettler, F.; Forst, D.; Hess, H. *Z. Naturforsch.* **1976**, *31b*, 897.

(15) $Cu_3(\mu_2\text{-}SPh)_3(Ph_3P)_4$: Dance, I. G.; Fitzpatrick, L. J.; Scudder, M. L. *J. Chem. Soc., Chem. Commun.* **1983**, 546.

(16) $[Cu_3(SCH_2CH_2S)_3]^{3-}$: Rao, Ch. Pulla; Dorfman, J. R.; Holm, R. H. *Inorg. Chem.* **1986**, *25*, 428.

(17) (a) $[Cu_3(S_4)_3]^{3-}$: Baumann, F.-W.; Bögge, H.; Römer, M.; Krickemeyer, E.; Schmitz, K. *Angew. Chem., Int. Ed. Engl.* **1984**, *23*, 632. (b) $[Cu_3(S_6)_3]^{3-}$: Müller, A.; Schimanski, U. *Inorg. Chim. Acta* **1983**, *77*, L187. In these complexes the bridging atoms are from polysulfide rather than thiolate ligands.

(18) $Cu_3(SPMe_3)_3Cl_3$: Tiethof, J. A.; Stalick, J. K.; Corfield, P. W. R.; Meek, D. W. *J. Chem. Soc., Chem. Commun.* **1972**, 1141. This is not a thiolate complex, but it does contain a $Cu_3[\mu_2\text{-}S(PMe)_3]_3$ ring structurally related to those in the preceding compounds.[12-17]

(19) Palermo, R. E.; Power, P. P.; Holm, R. H. *Inorg. Chem.* **1982**, *21*, 173.

N, 3.78; S, 9.00. Absorption spectrum (acetonitrile): λ_{max} (ϵ_M) 260 (29 000), 330 (6900), 1850 (210) nm.

$(Et_4N)_3[Fe_3(S\text{-}p\text{-}C_6H_4Me)_3Cl_6]$ (4b). The previous method was followed with use of $(Et_4N)(S\text{-}p\text{-}C_6H_4Me)$, giving a 71% yield. An analytical sample was obtained by recrystallization from acetonitrile. Anal. Calcd for $C_{45}H_{81}Cl_6Fe_3N_3S_3$: C, 47.39; H, 7.16; Cl, 18.65; Fe, 14.69; N, 3.68; S, 8.43. Found: C, 47.88; H, 6.94; Cl, 18.45; Fe, 15.14; N, 3.91; S, 8.97.

$(Et_4N)_3[Fe_3(SPh)_3Br_6]$ (4c). The procedure for $(Et_4N)_3[Fe_3(SPh)_3Cl_6]$ was followed with use of anhydrous $FeBr_2$, giving a 61% yield of dark brown crystals. An analytical sample was obtained by recrystallization from acetonitrile followed by drying in vacuo for 12 h at ambient temperature. Anal. Cald for $C_{42}H_{75}Br_6Fe_3N_3S_3$: C, 36.95; H, 5.54; Br, 35.12; Fe, 12.27; N, 3.08; S, 7.04. Found: C, 37.30; H, 5.60; Br, 34.64; Fe, 12.65; N, 3.62; S, 7.13.

$(Et_4N)_3[Fe_3(S\text{-}2,6\text{-}Me_2C_6H_3)_3Cl_6]\cdot 3MeCN$ (4d). Sodium 2,6-dimethylbenzenethiolate (1.6 g (10 mmol), from the thiol[20] and NaH in ether) was slurried in ~100 mL of acetonitrile, and 1.3 g (10 mmol) of anhydrous $FeCl_2$ was added. Unlike the previous preparations, reaction was not immediate. The reaction mixture was stirred for 30 min, 1.65 g (10 mmol) of Et_4NCl was added, and stirring was continued for another 30 min. The dark brown filtrate of the reaction mixture was reduced by about one-half in volume and was maintained overnight at −25 °C. The product was obtained at 2.5 g (57%) of green hexagonal crystals which very readily lost solvate molecules. This compound was not analyzed but was identified by ^1H NMR and an X-ray structural analysis (vide infra).

Collection and Reduction of X-ray Data. Single crystals of compounds **4a**, **4c**, **4d**, and **5** in Table I were obtained as follows: **4a** and **5**, slow cooling of acetonitrile/ether solutions to −25 °C; **4c** and **4d**, ether diffusion in acetonitrile solutions at ambient temperature. Crystals of all compounds except **4d** were mounted in glass capillaries, which were sealed under dinitrogen. Triply solvated **4d** forms crystals that are stable in the mother liquor but rapidly lose solvent when removed therefrom. Considerable difficulty was encountered in obtaining a suitable crystal. Microscopic examination showed that the crystals fractured very easily. Rotation and axial photos were taken of about 20 crystals, one of which was marginally suitable. This was suspended in an epoxy resin, and the crystal was mounted on a glass fiber with an adhesive. All diffraction experiments were performed at ambient temperature on a Nicolet R3m or P3F automated four-circle diffractometer. For compounds **4a**, **4c**, and **4d**, a Mo source equipped with a graphite monochromator was employed. For compound **5**, both Mo (ω scans) and Cu ($\theta/2\theta$ scans) data sets were collected by using the indicated X-ray sources. The Cu data set was the more precise and was used for the structure solution and refinement. Final orientation matrices and cell parameters were obtained from a least-squares fit of 25 machine-centered reflections ($20 \le 2\theta \le 25°$ for **4a**, $12 \le 2\theta \le 25°$ for **4d**, $13 \le 2\theta \le 23°$ for **4c**, $25 \le 2\theta \le 50°$ for **5**). The crystal and machine parameters are summarized in Table I. The intensities of three check reflections were monitored every 123 reflections or less; no significant decay was seen over the course of data collection. Data for all compounds except **4d** were collected by the $\theta/2\theta$ technique. Fast ω scans were used for **4d** since the highly solvated crystals were not stable for more than several days. The programs XTAPE and XEMP from the SHELXTL program package (Nicolet XRD Corp., Madison, WI) were used for data processing and empirical absorption correction, respectively. The latter was applied to all data sets.

Structure Solution and Refinement. The SHELXTL package was employed throughout for compound **4a**, with the direct methods program SOLV used to locate the heavy atoms. For compounds **4c**, **4d**, and **5** MULTAN[21] was used to find the heavy atoms. These three compounds were refined with CRYSTALS.[22] For all compounds the remaining nonhydrogen atoms were found by difference Fourier maps, with intervening rounds of least-squares refinement. Atom scattering factors were taken from a standard source.[23] Hydrogen atoms at a C–H distance of 0.96 Å were included in all refinements. For compound **4a** hydrogen atom thermal parameters were fixed at 1.2× that of the bonded carbon atom, and phenyl groups were treated as rigid bodies. For compounds **4c**, **4d**, and **5**, hydrogen thermal parameters were fixed at 0.22 Å^2, phenyl groups were treated as semirigid bodies, and cations were restrained by the method of additional observational equations.[24] Refinement was carried out in a cascade fashion, with large-block approximations to the least-squares matrix. Unique crystal data and final R factors are given in Table I. Individual structure refinements are briefly described.

Table II. Atom Coordinates (×10^4) of $(Et_4N)_3[Fe_3(SPh)_3Cl_6]$

atom	x	y	z
Fe(1)	0	10165 (1)	2500
Fe(2)	976 (1)[a]	7353 (1)	2947 (1)
S(1)	798 (1)	9070 (1)	2883 (1)
S(2)	0	6787 (2)	2500
Cl(1)	28 (1)	11089 (1)	1472 (1)
Cl(2)	1438 (1)	6901 (2)	2114 (1)
Cl(3)	1456 (1)	6807 (1)	4194 (1)
C(1*s*1)	1445 (3)	9766 (4)	3242 (3)
C(2*s*1)	1984 (3)	9315 (6)	3522 (5)
C(3*s*1)	2498 (3)	9834 (7)	3808 (6)
C(4*s*1)	2480 (3)	10853 (7)	3804 (5)
C(5*s*1)	1953 (4)	11326 (6)	3556 (5)
C(6*s*1)	1442 (3)	10796 (5)	3276 (4)
C(1*s*2)	0	5478 (6)	2500
C(2*s*2)	508 (4)	4944 (5)	2725 (5)
C(3*s*2)	514 (4)	3918 (5)	2720 (6)
C(4*s*2)	0	3405 (8)	2500
N(1)	3331 (3)	5294 (4)	4138 (3)
C(1*n*1)	3743 (4)	5734 (7)	4951 (5)
C(2*n*1)	4328 (4)	6121 (9)	5022 (5)
C(3*n*1)	3263 (4)	6120 (9)	3544 (6)
C(4*n*1)	2965 (4)	7043 (7)	3636 (7)
C(5*n*1)	3691 (5)	4574 (8)	3932 (6)
C(6*n*1)	3730 (10)	3583 (9)	4512 (8)
C(7*n*1)	2821 (6)	5015 (11)	4276 (8)
C(8*n*1)	2392 (6)	4579 (10)	3401 (8)
N(2)[b]	0	5000	5000
C(1*n*2)	453 (7)	4779 (15)	4566 (9)
C(5*n*2)	−217 (12)	4143 (18)	5217 (16)
C(2*n*2)	752 (9)	3813 (19)	4843 (9)
C(3*n*2)	208 (12)	4092 (29)	5400 (17)
C(6*n*2)	−429 (8)	4767 (15)	4133 (10)
C(4*n*2)	−823 (7)	3973 (14)	4129 (10)

[a] Estimated standard deviation in parentheses in this and succeeding tables. [b] Disordered cation.

(a) $(Et_4N)_3[Fe_3(SPh)_3Cl_6]$. The systematic absences hkl ($h + k = 2n + 1$), $h0l$ ($h = 2n + 1$, $l = 2n + 1$), and $0k0$ ($k = 2n + 1$) correspond to the space groups Cc (no. 9) or $C2/c$ (no. 15). Successful refinement proved the latter to be correct. The asymmetric unit consists of 0.5 anion and 1.5 cations. The anion lies on a twofold axis and exhibits no disorder. One cation is located at a general position and is unexceptional; however, the nitrogen atom of a second cation occupies an inversion center, necessitating a disorder of methylene carbon atoms. These atoms were refined to occupancies of 0.57 and 0.43 for the pair C(1)N(2) and C(5)N(2) and 0.60 and 0.40 for the pair C(3)N(2) and C(6)N(2). All non-hydrogen atoms were refined anisotropically.

(b) $(Et_4N)_3[Fe_3(S\text{-}2,6\text{-}Me_2C_6H_3)_3Cl_6]\cdot 3MeCN$. The systematic absences $h0l$ ($h + l = 2n + 1$) and $0k0$ ($k = 2n + 1$) uniquely define the space group as $P2_1/n$ (no. 14, equivalent positions $\pm(x,y,z;\ ^1/_2 - x,\ ^1/_2 + y,\ ^1/_2 - z)$). The asymmetric unit contains one anion, three cations, and three solvate molecules. The anion and two cations show no disorder, but the third cation was found to have two disordered methylene carbon atoms (relative occupancies 0.66 and 0.33). One solvate molecule had thermal parameters sufficiently large to indicate disorder, but no suitable model for the disorder was found. Heavy atoms were refined anisotropically; carbon and nitrogen atoms were described isotropically.

(c) $(Et_4N)_3[Fe_3(SPh)_3Br_6]\cdot MeCN$. The systematic absences $hh\bar{2}hl$ ($l = 2n + 1$) and $000l$ ($l = 2n + 1$) (using hexagonal axes $hkil$ where $i = -(h + k)$) correspond to the hexagonal space groups $P6_3mc$ (no. 186), $P\bar{6}2c$ (no. 190), and $P6_3/mmc$ (no. 194). Direct methods and subsequent refinement proved that $P\bar{6}2c$ is the correct space group. The asymmetric unit consists of $^1/_6$ anion, $^1/_2$ cation, and $^1/_6$ solvate molecule. The cation and anion are not disordered. The nitrogen atom of the solvate molecule lies in a mirror plane, and the carbon atom positions were modeled in terms of disorder over two positions on each side of this plane. All non-hydrogen atoms except those of the solvate molecule were refined anisotropically.

(d) $(Et_4N)_2[Fe_4(SCH_2Ph)_6Br_4]$. Crystals of this compound are triclinic with possible space groups $P1$ (no. 1) or $P\bar{1}$ (no. 2). Intensity statistics favored the centrosymmetric space group, and this choice was confirmed

(20) Campaigne, E.; Osborn, S. W. *J. Org. Chem.* **1957**, *22*, 561.
(21) *MULTAN-80, A System of Computer Programs for the Automatic Solution of Crystal Structures from X-ray Diffraction Data*; Main, P., Fiske, S. J., Hull, S. E., Lessinger, L., Germain, G., Declercq, J.-P., Woolfson, M. M.; Universities of York and Louvain, 1980.
(22) Watkin, D. J.; Carruthers, J. R. *CRYSTALS Users Manual*; Chemical Crystallography Laboratory: Oxford University, 1984.
(23) Cromer, D. T.; Waber, J. T. *International Tables for X-ray Crystallography*; Kynoch Press: Birmingham, England, 1974; Vol. IV.
(24) Waser, J. *Acta Crystallogr.* **1963**, *16*, 1091.

Table III. Atom Coordinates ($\times 10^4$) of $(Et_4N)_3[Fe_3(S\text{-}2,6\text{-}Me_2C_6H_3)_3Cl_6]\cdot 3MeCN$

atom	x	y	z	atom	x	y	z
Fe(1)	1228 (2)	2337 (1)	9561 (1)	C(42)	3173 (19)	2505 (18)	3158 (9)
Fe(2)	4195 (2)	2334 (1)	9678 (1)	C(43)	3054 (14)	2339 (13)	5034 (8)
Fe(3)	2665 (2)	3693 (1)	10778 (1)	C(44)	2269 (19)	2348 (18)	5486 (9)
S(1)	2706 (3)	2010 (2)	9514 (3)	C(45)	2084 (11)	1859 (8)	4148 (15)
S(2)	3876 (3)	3129 (2)	10396 (2)	C(46)	2614 (16)	1281 (7)	4157 (13)
S(3)	1476 (3)	3122 (2)	10316 (2)	C(47)	2187 (13)	2986 (7)	4231 (14)
Cl(1)	366 (4)	1614 (3)	10003 (4)	C(48)	2790 (18)	3503 (7)	4432 (16)
Cl(2)	712 (5)	2668 (3)	8572 (2)	C(141)	2378 (14)	2522 (20)	3605 (8)
Cl(3)	4830 (4)	2672 (3)	8749 (2)	C(143)	1914 (12)	2338 (22)	4781 (10)
Cl(4)	4993 (4)	1594 (3)	10186 (4)	C(145)	3238 (14)	1797 (7)	4329 (22)
Cl(5)	2644 (4)	3654 (2)	11894 (2)	C(147)	3301 (15)	2922 (8)	4550 (21)
Cl(6)	2663 (4)	4640 (2)	10374 (3)	N(5)	232 (8)	25 (5)	2048 (6)
C(11)	2686 (6)	1307 (4)	9068 (8)	C(51)	705 (11)	136 (10)	1396 (7)
C(12)	2717 (6)	1300 (7)	8389 (8)	C(52)	42 (17)	128 (16)	824 (9)
C(13)	2703 (6)	753 (9)	8064 (7)	C(53)	-307 (10)	-565 (6)	2016 (9)
C(14)	2651 (6)	226 (7)	8420 (10)	C(54)	284 (15)	-1102 (7)	1894 (14)
C(15)	2615 (6)	234 (6)	9099 (10)	C(55)	-442 (10)	528 (7)	2188 (10)
C(16)	2634 (6)	780 (8)	9425 (7)	C(56)	13 (17)	1134 (7)	2208 (17)
C(17)	2782 (16)	1847 (11)	8023 (12)	C(57)	969 (9)	1 (8)	2592 (7)
C(18)	2569 (17)	753 (12)	10173 (13)	C(58)	567 (14)	-67 (12)	3261 (8)
C(21)	4880 (4)	3458 (5)	10749 (6)	N(6)	5477 (7)	89 (5)	7875 (5)
C(22)	5226 (8)	3254 (5)	11346 (6)	C(61)	5025 (10)	710 (6)	7845 (9)
C(23)	5992 (8)	3514 (6)	11611 (5)	C(62)	5664 (15)	1200 (7)	8066 (13)
C(24)	6402 (7)	3979 (6)	11285 (7)	C(63)	4757 (9)	-382 (7)	7693 (10)
C(25)	6056 (8)	4181 (5)	10688 (7)	C(64)	5139 (17)	-1011 (7)	7687 (16)
C(26)	5289 (8)	3922 (5)	10421 (5)	C(65)	5878 (10)	-37 (9)	8566 (6)
C(27)	4775 (14)	2736 (10)	11702 (10)	C(66)	5164 (16)	-38 (14)	9077 (9)
C(28)	4963 (13)	4157 (9)	9743 (10)	C(67)	6262 (8)	63 (8)	7401 (7)
C(31)	453 (4)	3496 (6)	10524 (8)	C(68)	5943 (14)	127 (12)	6692 (7)
C(32)	-2 (10)	3322 (5)	11075 (7)	N(7)[b]	2440 (15)	1156 (11)	2183 (12)
C(33)	-782 (9)	3615 (7)	11234 (7)	C(71)	2487 (14)	1521 (10)	1792 (11)
C(34)	-1099 (8)	4076 (7)	10839 (9)	C(72)	2602 (16)	2005 (11)	1327 (13)
C(35)	-650 (10)	4247 (5)	10285 (8)	N(8)[b]	7273 (24)	392 (18)	3115 (18)
C(36)	131 (10)	3956 (6)	10126 (6)	C(81)	7541 (20)	832 (15)	3389 (16)
C(37)	369 (18)	2783 (13)	11500 (13)	C(82)	7822 (18)	1323 (13)	3788 (14)
C(38)	564 (15)	4153 (11)	9508 (12)	N(9)[b]	7883 (34)	1345 (23)	1326 (25)
N(4)[a]	2708 (8)	2392 (6)	4316 (7)	C(91)	7229 (59)	1577 (40)	1660 (45)
C(41)	3507 (11)	2390 (13)	3855 (10)	C(92)	7286 (74)	2012 (52)	2016 (56)

[a] Disordered cation. [b] Acetonitrile solvate molecule.

Table IV. Atom Coordinates ($\times 10^4$) of $(Et_4N)_3[Fe_3(SPh)_3Br_6]\cdot MeCN$

atom	x	y	z
Br(1)	810 (1)	7124 (1)	1405.5 (8)
Fe(1)	1690 (2)	6969 (2)	2500
S(1)	1717 (3)	5300 (4)	2500
C(1)	349 (9)	4154 (8)	2500
C(2)	-543 (10)	4332 (10)	2500
C(3)	-1613 (9)	3435 (11)	2500
C(4)	-1801 (10)	2359 (11)	2500
C(5)	-910 (11)	2178 (9)	2500
C(6)	159 (10)	3077 (9)	2500
N(1)	3633 (8)	0	0
C(10)	3782 (13)	-957 (10)	295 (7)
C(11)	4203 (20)	-1418 (16)	-299 (10)
C(12)	2797 (10)	-414 (11)	-643 (5)
C(13)	1670 (11)	-1334 (15)	-396 (9)
N(2)[a]	0	0	2500
C(20)	0	0	1867 (3)
C(21)	0	0	1069 (4)

[a] Acetonitrile solvate.

by successful solution and refinement of the structure. The asymmetric unit is very large, containing two anions and four cations; no disorder is present. All heavy atoms and benzyl methylene carbon atoms were refined anisotropically. All other non-hydrogen atoms were refined isotropically.

Atom coordinates for compounds **4a**, **4c**, **4d**, and **5** are compiled in Tables II–V.[25]

Other Physical Measurements. ^1H NMR spectra were measured with a Bruker WM-300 spectrometer operating at 300 MHz. Chemical shifts are quoted vs. Me_4Si internal reference. Magnetic susceptibilities in the solid state were determined on a SHE 905 SQUID Magnetometer. Samples were sealed and weighed in previously calibrated containers. Several runs with different containers and different samples of the same compound were made to ensure reproducibility of the results. Susceptibilities in CD_3CN solution were measured by the standard NMR method with Me_4Si reference signals. Changes in solution densities with temperature were taken into account; the solvent susceptibility is the value determined by Gerger et al.[26a] Diamagnetic corrections were applied.[26b] All measurements were performed under anaerobic conditions.

Results and Discussion

Preparation of Compounds. Reactions 1–4 in Figure 1 afford products with the same RS^-:Fe(II) ratios as the reactant stoichiometries, thereby providing a straightforward means of synthesis of the four types of iron(II) thiolate complexes **1**–**4**. $[Fe_3(SPh)_3Cl_6]^{3-}$ was originally discovered[4] as a consequence of systematic variations of these stoichiometries, intended to reveal the existence of all possible iron(II) thiolates. Reaction 5, a generalized version of reaction 4, gives the indicated products,

$$3FeX_2 + 3(Et_4N)(SR) \xrightarrow{MeCN} (Et_4N)_3[Fe_3(SR)_3X_6] \quad (5)$$

4a: X = Cl, R = Ph
4b: X = Cl, R = *p*-C_6H_4Me (*p*-tol)
4d: X = Cl, R = 2,6-$Me_2C_6H_3$ (Me_2Ph)
4c: X = Br, R = Ph

(25) See paragraph at the end of this article concerning supplementary material available.

(26) (a) Gerger, W.; Mayer, U.; Gutman, V. *Monatsh. Chem.* **1977**, *108*, 417. (b) Landolt-Bornstein, *Numerical Data and Functional Relationships in Science and Technology*; König, E., Ed.; Springer-Verlag: Berlin, 1966; Vol. II-2, "Magnetic Properties of Coordination and Organometallic Transition Metal Compounds."

Table V. Positional Parameters for the $Fe_4(SC)_6Br_4$ Portion of $[Fe_4(SCH_2Ph)_6Br_4]^{2-}$

atom	x	y	z
Fe(1)	8289 (2)	−33 (2)	5823.2 (5)
Fe(2)	6326 (2)	−2638 (2)	6119.6 (6)
Fe(3)	8563 (2)	−376 (2)	6700.1 (5)
Fe(4)	5920 (2)	−157 (2)	6342.8 (6)
Br(1)	9371 (2)	548 (2)	5392.0 (4)
Br(2)	5433 (2)	−4547 (2)	5991.0 (5)
Br(3)	9978 (2)	211 (2)	7148.6 (5)
Br(4)	4674 (2)	692 (2)	6460.2 (5)
S(1)	7135 (4)	−1874 (4)	5681 (1)
S(2)	9532 (4)	61 (4)	6258 (1)
S(3)	6847 (4)	549 (4)	5906 (1)
S(4)	7571 (4)	−2224 (4)	6578 (1)
S(5)	7005 (4)	−36 (4)	6810 (1)
S(6)	4955 (4)	−2008 (4)	6218 (1)
Fe(11)	8919 (2)	3809 (2)	1548.3 (6)
Fe(12)	6941 (2)	2603 (2)	781.3 (6)
Fe(13)	7811 (2)	5499 (2)	1084.0 (6)
Fe(14)	5685 (2)	3188 (2)	1472.0 (6)
Br(11)	10553 (2)	4017 (2)	1898.0 (5)
Br(12)	6612 (2)	1426 (2)	303.1 (5)
Br(13)	8364 (2)	7332 (2)	998.7 (5)
Br(14)	4129 (2)	2758 (2)	1794.1 (5)
S(11)	8380 (4)	2470 (4)	1124 (1)
S(12)	9445 (4)	5374 (4)	1314 (1)
S(13)	7203 (4)	3053 (4)	1771 (1)
S(14)	7347 (4)	4287 (4)	632 (1)
S(15)	5991 (4)	4757 (4)	1255 (1)
S(16)	5238 (4)	1989 (4)	1020 (1)
C(10)	8103 (15)	−2499 (15)	5605 (3)
C(20)	10848 (15)	1346 (16)	6334 (5)
C(30)	7554 (17)	1993 (14)	6056 (4)
C(40)	8659 (16)	−2707 (16)	6499 (4)
C(50)	7500 (19)	1319 (16)	7021 (4)
C(60)	4140 (15)	−2244 (18)	5831 (4)
C(110)	9564 (18)	2862 (17)	874 (5)
C(120)	10315 (16)	6498 (15)	1612 (4)
C(130)	7334 (18)	3855 (16)	2145 (4)
C(140)	8649 (17)	4603 (17)	441 (4)
C(150)	5834 (17)	5683 (16)	1567 (4)
C(160)	5183 (18)	716 (15)	1141 (6)

[a] Anion 1: Fe(1–4), Br(1–4), S(1–6), C(10–60). All other atoms belong to anion 2.

all of the cyclic type **4**, in good yield. Ligands R and X were selected to provide a useful NMR spectral probe (*p*-tol) and to introduce steric features (Br, Me_2Ph) that might affect conformations of $Fe_3(SR)_3$ rings and relative orientations of these and phenyl rings. Structural results are first considered.

Structures of $[Fe_3(SR)_3X_6]^{3-}$. Crystals of three compounds containing anions of this composition (Table I) consist of discrete anions, cations, and, in two cases, solvate molecules. When not affected by disorder, dimensions of the latter two components are unexceptional and are not described. Poor crystal quality was encountered with $(Et_4N)_3[Fe_3(S\text{-}Me_2Ph)_3Cl_6]\cdot 3MeCN$, but the data were adequate to define heavy atom positions satisfactorily and to determine phenyl ring orientations. Anion structures are depicted in Figures 2–4, and interatomic distances and angles are collected in Table VI. As seen from the number of independent parameters per complex, imposed symmetry varies from none with $[Fe_3(S\text{-}Me_2Ph)_3Cl_6]^{3-}$, to C_2 with $[Fe_3(SPh)_3Cl_6]^{3-}$ where the symmetry axis contains Fe(1) and S(2), to C_{3h} with $[Fe_3(SPh)_3Br_6]^{3-}$. Because of its high symmetry, the last complex has only eight independent distances and angles involving directly bonded atoms in the $Fe_3(SC)_3Br_6$ portion of the molecule.

The three complexes contain $Fe_3(\mu_2\text{-}SR)_3$ rings with nearly or precisely planar Fe_2SC and distorted tetrahedral FeS_2X_2 units (X = Cl^-, Br^-). All distances and angles of a given type within the rings are practically constant, as are angles (Fe–S–C, X–Fe–X, S–Fe–X) external to the ring. Distances of Fe–S bonds are ordinary when compared to Fe-(μ_2-SR) mean values in $[Fe_2(SEt)_6]^{2-}$ (**2**, R = Et; 2.375 (1) Å),[6] $[Fe_4(SEt)_{10}]^{2-}$ (**3**, R = Et; 2.354 (9) Å),[6] $[Fe_4(SPh)_{10}]^{2-}$ (**3**, R = Ph; 2.368 (14) Å),[3] and

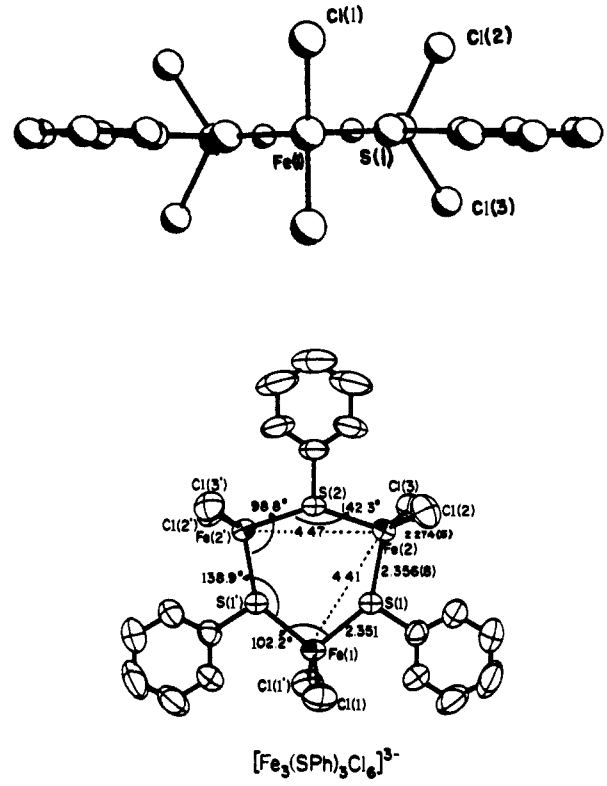

Figure 2. Two views of the structure of $[Fe_3(SPh)_3Cl_6]^{3-}$. In the top view atoms are represented by spheres of arbitrary radii and in the bottom view by 50% probability ellipsoids. Selected interatomic distances and angles and the atom labeling scheme are given.

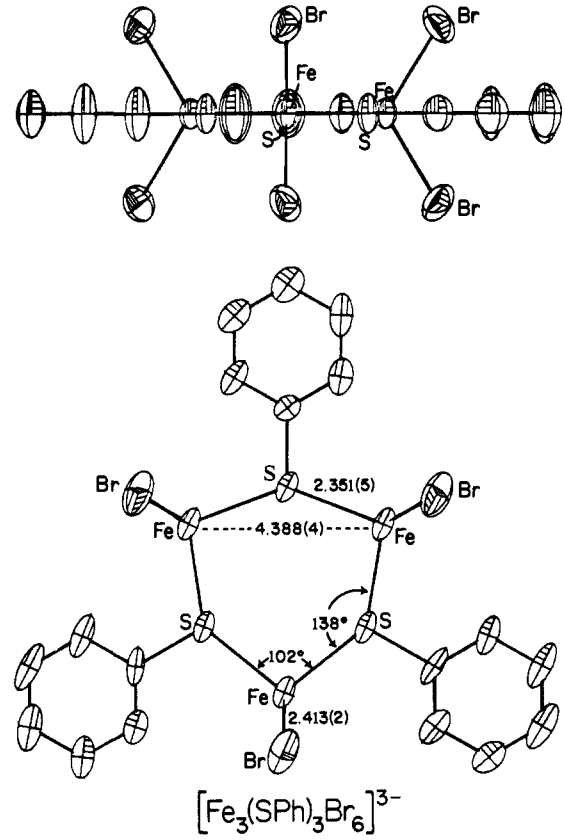

Figure 3. Two views of the structure of $[Fe_3(SPh)_3Br_6]^{3-}$ in which 50% probability ellipsoids, selected interatomic distances and angles, and the atom labeling scheme are shown.

$[Fe_4(\mu_2\text{-}SPh)_6Cl_4]^{2-}$ (2.362 (15) Å).[27] Similarly, the Fe–X bond lengths are normal when taken with mean values in $[FeCl_4]^{2-}$

Table VI. Selected Interatomic Distances (Å) and Angles (deg) in $[Fe_3(SPh)_3Cl_6]^{3-}$ (**4a**), $[Fe_3(S\text{-}2,6\text{-}Me_2C_6H_3)_3Cl_6]^{3-}$ (**4d**), and $[Fe_3(SPh)_3Br_6]^{3-}$ (**4c**)

4a		4d		4c	
		Fe–S			
Fe(1)–S(1)	2.351 (2)	Fe(1)–S(1)	2.349 (6)	Fe–S	2.351 (5)
Fe(2)–S(1)	2.352 (2)	Fe(1)–S(3)	2.361 (5)		
Fe(2)–S(2)	2.365 (2)	Fe(2)–S(1)	2.373 (6)		
mean	2.356 (8)	Fe(2)–S(2)	2.365 (5)		
		Fe(3)–S(2)	2.369 (5)		
		Fe(3)–S(3)	2.376 (5)		
		mean	2.366 (10)		
		Fe–X			
Fe(1)–Cl(1)	2.271 (3)	Fe(1)–Cl(1)	2.278 (4)	Fe–Br	2.413 (2)
Fe(2)–Cl(2)	2.272 (3)	Fe(1)–Cl(2)	2.273 (4)		
Fe(2)–Cl(3)	2.280 (2)	Fe(2)–Cl(3)	2.279 (4)		
mean	2.274 (5)	Fe(2)–Cl(4)	2.281 (4)		
		Fe(3)–Cl(5)	2.285 (4)		
		Fe(3)–Cl(6)	2.276 (4)		
		mean	2.279 (4)		
		Fe···Fe			
Fe(1)···Fe(2)	4.407 (4)	Fe(1)···Fe(2)	4.471 (4)	Fe···Fe	4.388 (4)
Fe(2)···Fe(2′)	4.473 (3)	Fe(1)···Fe(3)	4.450 (4)		
		Fe(2)···Fe(3)	4.463 (4)		
		S–C			
S(1)–C(1)	1.757 (6)	S(1)–C(11)	1.816 (6)	S–C	1.780 (11)
S(2)–C(1)	1.766 (8)	S(2)–C(21)	1.813 (6)		
		S(3)–C(31)	1.815 (6)		
		mean	1.815 (2)		
		S–Fe–S			
S(1)–Fe(1)–S(1′)	102.2 (1)	S(1)–Fe(1)–S(3)	97.2 (2)	S–Fe–S	101.8 (2)
S(1)–Fe(2)–S(2)	98.8 (1)	S(1)–Fe(2)–S(2)	96.4 (2)		
		S(2)–Fe(3)–S(3)	99.3 (2)		
		Fe–S–Fe			
Fe(1)–S(1)–Fe(2)	138.9 (1)	Fe(1)–S(1)–Fe(2)	142.5 (2)	Fe–S–Fe	138.2 (2)
Fe(2)–S(2)–Fe(2′)	142.3 (1)	Fe(2)–S(2)–Fe(3)	141.0 (2)		
		Fe(1)–S(3)–Fe(3)	139.9 (2)		
		Fe–Fe–Fe			
Fe(2)–Fe(1)–Fe(2′)	61.0 (1)	Fe(2)–Fe(1)–Fe(3)	60.0 (1)	Fe–Fe–Fe	60.0
Fe(1)–Fe(2)–Fe(2′)	59.5 (1)	Fe(1)–Fe(2)–Fe(3)	59.8 (1)		
		Fe(1)–Fe(3)–Fe(2)	60.2 (1)		
		Fe–S–C			
Fe(1)–S(1)–C(1)	108.7 (2)	Fe(1)–S(1)–C(11)	106.7 (4)	Fe–S–C	110.5 (4)
Fe(2)–S(1)–C(1)	112.4 (2)	Fe(2)–S(1)–C(11)	109.8 (4)		
Fe(2)–S(2)–C(1)	108.8 (2)	Fe(2)–S(2)–C(21)	111.8 (4)		
		Fe(3)–S(2)–C(21)	107.1 (3)		
		Fe(1)–S(3)–C(31)	112.0 (4)		
		Fe(3)–S(3)–C(31)	107.2 (4)		
		X–Fe–X			
Cl(1)–Fe(1)–Cl(1′)	109.0 (1)	Cl(1)–Fe(1)–Cl(2)	113.5 (3)	Br–Fe–Br	112.1 (1)
Cl(2)–Fe(2)–Cl(3)	112.1 (1)	Cl(3)–Fe(2)–Cl(4)	113.2 (3)		
		Cl(5)–Fe(3)–Cl(6)	113.5 (2)		
		S–Fe–X			
S(1)–Fe(1)–Cl(1)	109.0 (1)	S(1)–Fe(1)–Cl(1)	110.3 (3)	S–Fe–Br	110.5 (1)
S(1)–Fe(1)–Cl(1′)	111.3 (1)	S(1)–Fe(1)–Cl(2)	111.5 (3)		
S(1)–Fe(2)–Cl(2)	111.0 (1)	S(1)–Fe(2)–Cl(3)	113.6 (2)		
S(1)–Fe(2)–Cl(3)	112.9 (1)	S(1)–Fe(2)–Cl(4)	109.1 (3)		
S(2)–Fe(2)–Cl(2)	111.4 (1)	S(2)–Fe(2)–Cl(3)	111.4 (2)		
S(2)–Fe(2)–Cl(3)	110.0 (1)	S(2)–Fe(2)–Cl(4)	112.1 (3)		
		S(2)–Fe(3)–Cl(5)	109.9 (2)		
		S(2)–Fe(3)–Cl(6)	111.7 (2)		
		S(3)–Fe(1)–Cl(1)	110.6 (3)		
		S(3)–Fe(1)–Cl(2)	112.7 (2)		
		S(3)–Fe(3)–Cl(5)	110.3 (2)		
		S(3)–Fe(3)–Cl(6)	111.3 (2)		

(2.292 (2) Å),[28] $[Fe_4(SPh)_6Cl_4]^{2-}$ (2.254 (3) Å[27]), and $[Fe_4(SCH_2Ph)_6Br_4]^{2-}$ (vide infra).

Two interrelated structural features of the three cyclic complexes are remarkable: near or exact planarity of the $Fe_3(SR)_3$ rings and extraordinarily large internal angles and planar stereochemistry at sulfur. In $[Fe_3(SPh)_3Br_6]^{3-}$ (Figure 3) ring planarity and dihedral angles of 0° or 90° between the phenyl groups and the Fe_3S_3 plane are required by the imposed C_{3h} symmetry. The 0° angles arrangement is found, all four rings being coplanar. The structure of $[Fe_3(SPh)_3Cl_6]^{3-}$ (Figure 2) approaches this ar-

(27) Coucouvanis, D.; Kanatzidis, M.; Simhon, E.; Baenziger, N. C. *J. Am. Chem. Soc.* **1982**, *104*, 1874.
(28) Lauher, J. W.; Ibers, J. A. *Inorg. Chem.* **1975**, *14*, 348.

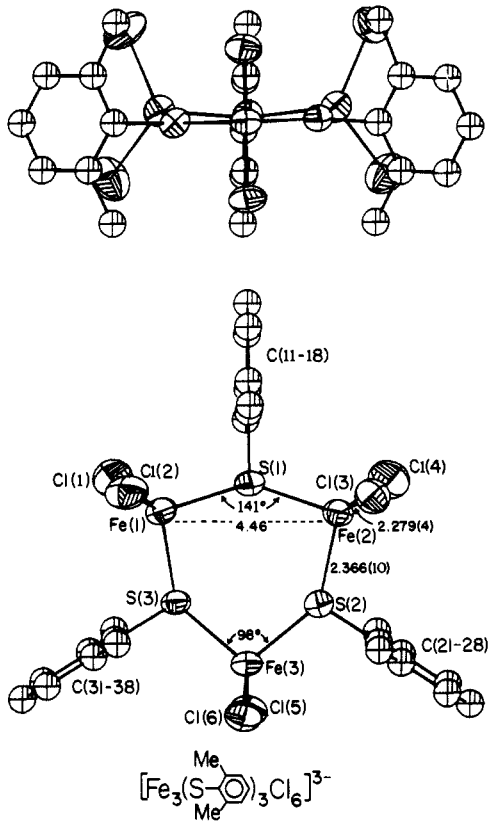

Figure 4. Two views of the structure of $[Fe_3(SMe_2Ph)_3Cl_6]^{3-}$; the same information as in Figure 3 is given, except that C atoms are shown as spheres of arbitrary radius.

Table VII. Atom Deviations (Å) from Unweighted Fe_3S_3 Least-Squares Planes and Dihedral Angles (deg) with Phenyl Rings

$[Fe_3(SPh)_3Cl_6]^{3-}$		$[Fe_3(S\text{-}Me_2Ph)_3Cl_6]^{3-}$	
atom	dev	atom	dev
Fe(1)	0	Fe(1)	0.118
Fe(2)	-0.016	Fe(2)	0.099
Fe(2′)	0.016	Fe(3)	0.023
S(1)	0.019	S(1)	-0.154
S(1′)	-0.019	S(2)	-0.032
S(2)	0	S(3)	-0.054
ring	angle[a]	ring	angle[a]
S(1)Ph	3.2	S(1)Ph	87.9
S(2)Ph	1.4	S(2)Ph	89.4
		S(3)Ph	88.6

[a] Between Fe_3S_3 and C_6 rings.

rangement, but the imposed C_2 symmetry requires neither a planar central ring nor three equal dihedral angles of 0° or 90°. Nonetheless, the observed structure is the same in all significant details as that of $[Fe_3(SPh)_3Br_6]^{3-}$. The data in Table VII reveal atom deviations from a planar Fe_3S_3 ring of <0.02 Å and dihedral angle variances from 0° to ≲3°. In $[Fe_3(S\text{-}Me_2Ph)_3Cl_6]^{2-}$ (Figure 4) the three phenyl rings are rotated by nearly 90° out of the Fe_3S_3 least-squares plane. The central ring becomes slightly ruffled in the direction of a chair conformation, with the three Fe and three S atoms unsymmetrically positioned on opposites sides of the plane (Table VII).

The set of three structures in Table VI and Figures 2–4 was sought in order to identify any stereochemical effects of differently sized $Fe_3(SR)_3$ ring substitutents on, particularly, central ring planarity and coplanarity of the four rings. Pauling's estimates of van der Waals radii are 1.80 (Cl), 1.95 (Br), and 2.0 (Me) Å.[29]

(29) Pauling, L. *The Nature of the Chemical Bond*, 3rd ed.; Cornell University Press: Ithaca, New York, 1960; pp 257–264.

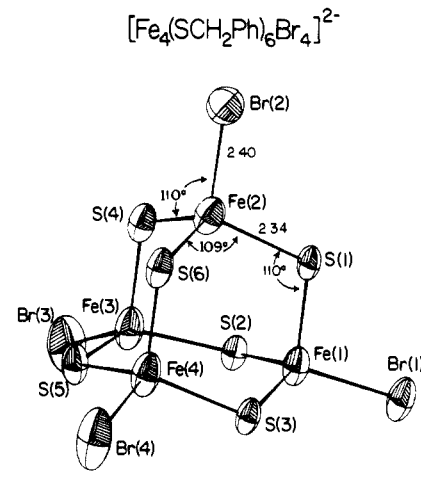

Figure 5. Structure of the $Fe_4S_6Br_4$ portion of $[Fe_4(SCH_2Ph)_6Br_4]^{2-}$, showing 50% probability ellipsoids, the atom labeling scheme, and selected distances and angles averaged under idealized T_d symmetry.

Evidently, the longer Fe–Br distance (2.413 (2) Å) offsets the larger Br radius such that the *o*-H atoms of phenyl groups in $[Fe_3(SPh)_3Br_6]^{3-}$ find minimum steric repulsion with Br atoms in a plane bisecting the Br–Fe–Br angle. The two $[Fe_3(SPh)_3X_6]^{3-}$ complexes have corresponding conformations. In the pair $[Fe_3(SR)_3Cl_6]^{3-}$, with indistinguishable Fe–Cl bond lengths of 2.28 Å, the *o*-Me groups of the R = Me_2Ph substituent minimize contact with Cl atoms in the conformation with phenyl rings perpendicular to the central ring. This conclusion is supported by calculations of van der Waals repulsion energies as a function of dihedral angle formed by Fe_3S_3 and phenyl rings. By use of the program MODEL,[30] a deep energy minimum is found at the observed perpendicular ring orientation. The significantly longer S–C distance (by ~0.05 Å) in $[Fe_3(SMe_2Ph)_3Cl_6]^{3-}$ may provide an additional means of alleviating Me···Cl interactions. For $[Fe_3(SPh)_3X_6]^{3-}$ shallow minima are found at 0° and 180° and are not decisive in rationalizing the coplanar structures.

The foregoing results, obtained with crystals having different packing arrangements and imposed anion site symmetries, suggest that the *$Fe_3(SR)_3$ rings have an intrinsic planar or near-planar conformational preference.* Further, this preference is not dependent on phenyl substituent orientation.

$[Fe_4(SCH_2Ph)_6Br_4]^{2-}$ (5). In order to broaden the scope of $[Fe_3(SR)_3X_6]^{3-}$ complexes and therewith provide additional information on substituent/property relationships, species with R = alkyl were sought in a number of attempts. In one case, using $FeBr_2$, $NaSCH_2Ph$, and Et_4NBr in acetonitrile and the stoichiometry of reaction 5, a dark brown crystalline product was isolated. Because this material could not be securely identified by any other means, an X-ray structural analysis was performed. (Use of $FeCl_2$, $NaSCH_2Ph$, and Et_4NCl in an analogous system gave $(Et_4N)_2[FeCl_4]$ as the only isolable product.) The compound was established to be $(Et_4N)_2[Fe_4(SCH_2Ph)_6Br_4]$, which crystallized in triclinic space group $P\bar{1}$ with four cations and two anions in the asymmetric unit. Both anions have the same adamantane-like structure **3** with bromide instead of thiolate as the terminal ligand. The heavy atom portion of anion 1 is set out in Figure 5; metric data for the two essentially isodimensional anions are collected in Table VIII. The structure, which is similar to that of $[Fe_4(SPh)_6Cl_4]^{2-}$,[27] contains a $Fe_4(\mu_2\text{-}S)_6$ cage formed from four Fe_3S_3 rings joined at common Fe(II) atoms, each of which is in a distorted tetrahedral coordination site. The large variability of S–Fe–S angles is typical of such cage structures[3,6,11,27] and reflects their easy deformability (induced in part by relative R group conformations) from idealized T_d symmetry.

In terms of composition and electronic properties but not conformations, the rings present in $[Fe_4(SR)_6X_4]^{2-}$ (X = Cl^-, Br^-), whose overall structures are similar, provide the closest approaches

(30) From the CHEMGRAF suite of programs.

Table VIII. Selected Interatomic Distances (Å) and Angles (deg) for $[Fe_4(SCH_2Ph)_6Br_4]^{2-}$

anion 1		anion 2	
		Fe–Br	
Fe(1)–Br(1)	2.398 (3)	Fe(11)–Br(11)	2.400 (3)
Fe(2)–Br(2)	2.407 (3)	Fe(12)–Br(12)	2.423 (3)
Fe(3)–Br(3)	2.393 (3)	Fe(13)–Br(13)	2.418 (3)
Fe(4)–Br(4)	2.419 (3)	Fe(14)–Br(14)	2.413 (3)
mean	2.404 (11)	mean	2.413 (10)
		Fe–S	
Fe(1)–S(1)	2.359 (5)	Fe(11)–S(11)	2.343 (5)
Fe(1)–S(2)	2.341 (5)	Fe(11)–S(12)	2.339 (5)
Fe(1)–S(3)	2.356 (5)	Fe(11)–S(13)	2.329 (5)
Fe(2)–S(1)	2.349 (5)	Fe(12)–S(11)	2.368 (5)
Fe(2)–S(4)	2.327 (5)	Fe(12)–S(14)	2.341 (5)
Fe(2)–S(6)	2.329 (5)	Fe(12)–S(16)	2.346 (5)
Fe(3)–S(2)	2.339 (5)	Fe(13)–S(12)	2.342 (5)
Fe(3)–S(4)	2.334 (5)	Fe(13)–S(14)	2.341 (5)
Fe(3)–S(5)	2.319 (6)	Fe(13)–S(15)	2.330 (5)
Fe(4)–S(3)	2.369 (5)	Fe(14)–S(13)	2.348 (5)
Fe(4)–S(5)	2.326 (5)	Fe(14)–S(15)	2.347 (5)
Fe(4)–S(6)	2.338 (5)	Fe(14)–S(16)	2.331 (5)
mean	2.340 (15)	mean	2.342 (10)
		Fe···Fe	
Fe(1)–Fe(2)	3.838 (3)	Fe(11)–Fe(12)	3.816 (3)
Fe(1)–Fe(3)	3.874 (3)	Fe(11)–Fe(13)	3.853 (3)
Fe(1)–Fe(4)	3.870 (3)	Fe(11)–Fe(14)	3.861 (3)
Fe(2)–Fe(3)	3.810 (3)	Fe(12)–Fe(13)	3.791 (3)
Fe(2)–Fe(4)	3.771 (3)	Fe(12)–Fe(14)	3.692 (3)
Fe(3)–Fe(4)	3.778 (3)	Fe(13)–Fe(14)	3.849 (4)
mean	3.82 (2)	mean	3.81 (6)
		S–C	
S(1)–C(10)	1.826 (17)	S(11)–C(110)	1.851 (18)
S(2)–C(20)	1.859 (19)	S(12)–C(120)	1.829 (18)
S(3)–C(30)	1.862 (18)	S(13)–C(130)	1.843 (18)
S(4)–C(40)	1.835 (17)	S(14)–C(140)	1.824 (18)
S(5)–C(50)	1.847 (20)	S(15)–C(150)	1.865 (18)
S(6)–C(60)	1.837 (18)	S(16)–C(160)	1.869 (20)
mean	1.84 (1)	mean	1.85 (2)
		Br–Fe–S	
Br(1)–Fe(1)–S(1)	105.1 (1)	Br(11)–Fe(11)–S(11)	115.3 (2)
Br(1)–Fe(1)–S(2)	109.6 (2)	Br(11)–Fe(11)–S(12)	107.4 (2)
Br(1)–Fe(1)–S(3)	117.6 (2)	Br(11)–Fe(11)–S(13)	111.9 (2)
Br(2)–Fe(2)–S(1)	108.4 (2)	Br(12)–Fe(12)–S(11)	108.4 (2)
Br(2)–Fe(2)–S(4)	107.7 (2)	Br(12)–Fe(12)–S(14)	106.1 (2)
Br(2)–Fe(2)–S(6)	110.9 (2)	Br(12)–Fe(12)–S(16)	108.2 (2)
Br(3)–Fe(3)–S(2)	108.0 (2)	Br(13)–Fe(13)–S(12)	108.0 (2)
Br(3)–Fe(3)–S(4)	114.7 (2)	Br(13)–Fe(13)–S(14)	115.2 (2)
Br(3)–Fe(3)–S(5)	110.1 (2)	Br(13)–Fe(13)–S(15)	111.2 (2)
Br(4)–Fe(4)–S(3)	107.8 (2)	Br(14)–Fe(14)–S(13)	106.4 (2)
Br(4)–Fe(4)–S(5)	106.8 (2)	Br(14)–Fe(14)–S(15)	110.0 (2)
Br(4)–Fe(4)–S(6)	114.2 (2)	Br(14)–Fe(14)–S(16)	113.5 (2)
mean	110.1	mean	110.1
		S–Fe–S	
S(1)–Fe(1)–S(2)	104.4 (2)	S(11)–Fe(11)–S(12)	103.7 (2)
S(1)–Fe(1)–S(3)	110.1 (2)	S(11)–Fe(11)–S(13)	96.0 (2)
S(2)–Fe(1)–S(3)	117.7 (2)	S(12)–Fe(11)–S(13)	122.3 (2)
S(1)–Fe(2)–S(4)	116.9 (2)	S(11)–Fe(12)–S(14)	116.8 (2)
S(1)–Fe(2)–S(6)	105.6 (2)	S(11)–Fe(12)–S(16)	107.4 (2)
S(4)–Fe(2)–S(6)	107.3 (2)	S(14)–Fe(12)–S(16)	109.7 (2)
S(2)–Fe(3)–S(4)	100.4 (2)	S(12)–Fe(13)–S(14)	100.5 (2)
S(2)–Fe(3)–S(5)	125.1 (2)	S(12)–Fe(13)–S(15)	124.9 (2)
S(4)–Fe(3)–S(5)	98.0 (2)	S(14)–Fe(13)–S(15)	96.2 (2)
S(3)–Fe(4)–S(5)	120.3 (2)	S(13)–Fe(14)–S(15)	120.4 (2)
S(3)–Fe(4)–S(6)	107.6 (2)	S(13)–Fe(14)–S(16)	106.2 (2)
S(5)–Fe(4)–S(6)	100.3 (2)	S(15)–Fe(14)–S(16)	100.4 (2)
mean	108.6	mean	108.7
		Fe–S–Fe	
Fe(1)–S(1)–Fe(2)	109.2 (2)	Fe(11)–S(11)–Fe(12)	108.2 (2)
Fe(1)–S(2)–Fe(3)	111.7 (2)	Fe(11)–S(12)–Fe(13)	110.8 (2)
Fe(1)–S(3)–Fe(4)	110.0 (2)	Fe(11)–S(13)–Fe(14)	111.3 (2)
Fe(2)–S(4)–Fe(3)	109.7 (2)	Fe(12)–S(14)–Fe(13)	108.1 (2)
Fe(3)–S(5)–Fe(4)	108.9 (2)	Fe(13)–S(15)–Fe(14)	110.8 (2)
Fe(2)–S(6)–Fe(4)	107.8 (2)	Fe(12)–S(16)–Fe(14)	104.3 (2)
mean	109.5	mean	108.9

to those in the $[Fe_3(SR)_3X_6]^{3-}$ set. In the latter, the Fe–S–Fe angles vary over the small interval 138.2 (2)–142.5 (2)°. These values stand in contrast to the ranges of bridge angles in the *chair*-type rings of $[Fe_4(SPh)_6Cl_4]^{2-}$ (109–115°)[27] and $[Fe_4(SCH_2Ph)_6Br_4]^{2-}$ (104–112°),[31] which are near the tetrahedral angle of 109.5°. In all adamantane-like cage complexes[3,6,11,27] the stereochemistry at μ_2-S atoms is nonplanar. The only prior examples of a planar M_2SC unit occurs in $Cu_2(\mu_2\text{-}SPh)_2(PPh_3)_4$, where it is considered to be enforced by phenyl group crowding over the faces of the molecule.[32] The large bridge angles at sulfur are approached or matched only by the external M–(μ_2-S)–M angles joining $M_4(\mu_2\text{-}S)_6$ cages in $[Zn_4(SPh)_8(MeOH)]_n$[33a] (140°) and $[Cd(SPh)_2]_n$[33b] (136). Dance et al.[15] have recognized a smooth relationship between bridge angle θ and the angle of inclination ϕ between the S–C vector and the M_2S plane in the fragment **6** of $M_3(\mu_2\text{-}SPh)_3$ cycles. With $\phi \simeq 0°$ and $\theta \simeq 140°$, the com-

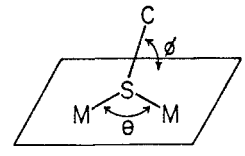

6

plexes $[Fe_3(SR)_3X_6]^{3-}$ lie at one extreme and are the only cases of six-membered rings with (near-) zero inclination angles. At the other extreme is $[Cu_4(SPh)_6]^{2-}$,[34] with chair-type rings, $\phi \simeq 63°$, and $\theta \simeq 74°$. For tetrahedral stereochemistry at sulfur $\phi = \theta/2 = 54.7°$. Although set by overall structure in the adamantane-like cage complexes, the chair-type conformations of Fe_3S_3 rings found there might appear to be a viable stereochemistry for $[Fe_3(SR)_3X_6]^{3-}$. Ring conformational preference in these complexes is investigated theoretically in a subsequent section.

Magnetic Properties. The magnetic behavior of the complexes $[Fe_3(SR)_3X_6]^{3-}$ is directly relevant to an interpretation of their ^1H NMR spectra and investigation of ring conformation in solution. The cyclic trimers and $[Fe_4(SR)_6X'_4]^{2-}$ (X' = RS^-, Cl^-, Br^-) provide a previously unavailable opportunity to assess magnetic coupling interactions in the bridge units Fe^{II}–(μ_2-S)–Fe^{II} as dependent on bridge angle θ at essential constancy of Fe–S distances. Values of θ are about 20° larger in $[Fe_3(SR)_3Cl_6]^{3-}$ than in $[Fe_4(SR)_6X'_4]^{2-}$ (compare, e.g., Tables VI and VIII). In view of the large Fe···Fe separations in the trinuclear and tetranuclear (3.8–4.0 Å) species, direct metal–metal interactions are expected to be small or negligible compared to those modulated by the bridging groups. The magnetic susceptibilities of $(Et_4N)_2[Fe(SEt)_4]$, $(Et_4N)_3[Fe_3(SPh)_3Cl_6]$, $(Me_4N)_2[Fe_4(SEt)_{10}]$, and $(n\text{-}Bu_4N)_2[Fe_4(S\text{-}p\text{-}tol)_{10}]$ were determined at 1.4- or 5–300 K in applied fields of 5–40 kG. Only $(Me_4N)_2[Fe_4(SEt)_{10}]$ showed a detectable field dependence of susceptibility at 5 K; data at ≥7 K were used in this case. All data refer to measurements at 5 kG.[25]

(a) $(Et_4N)_2[Fe(SEt)_4]$. This compound followed the Curie–Weiss law (eq 6) exactly at 5–302 K. Parameters were evaluated from linear regression analysis. The average magnetic moment was calculated from the relation $\mu_{av} = 2.828[\chi^M(T-\alpha)]^{1/2}$ and the g value from $g = \mu_{av}[S(S+1)]^{-1/2}$. These results define the

$$\chi^M = C/(T-\alpha) \qquad (6)$$

$$C = 3.289 \pm 0.007 \text{ emu K/mol} \qquad \alpha = 0.13 \pm 0.35 \text{ K}$$

$$\mu_{av} = 5.129 \pm 0.005 \qquad g = 2.090$$

properties of a magnetically dilute tetrahedral $[Fe(SR)_4]^{2-}$ com-

(31) Comparable bridge angles are found in $[Fe_4(SPh_4)_{10}]^{2-}$ (109–116°)[3] and $[Fe_4(SEt)_{10}]^{2-}$ (110–113°).[6]

(32) Dance, I. G.; Guerney, P. J.; Rae, A. D.; Scudder, M. L. *Inorg. Chem.* **1983**, *22*, 2883.

(33) (a) Dance, I. G. *J. Am. Chem. Soc.* **1980**, *102*, 3445. (b) Craig, D.; Dance, I. G.; Garbutt, R. *Angew. Chem., Int. Ed. Engl.* **1986**, *25*, 165.

(34) (a) Coucouvanis, D.; Murphy, C. N.; Kanodia, S. K. *Inorg. Chem.* **1980**, *19*, 2993. (b) Dance, I. G.; Bowmaker, G. A.; Clark, G. R.; Seadon, J. K. *Polyhedron* **1983**, *2*, 1031.

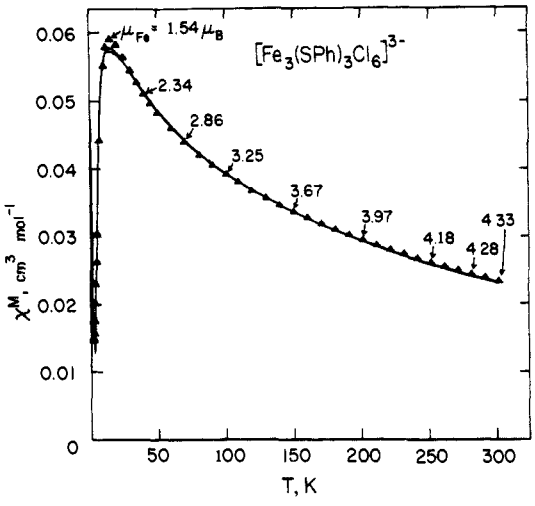

Figure 6. Temperature dependence of the molar magnetic susceptibility of $(Et_4N)_3[Fe_3(SPh)_3Cl_6]$. The solid lines are theoretical fits to the data with use of the parameters in Table IX. Values of $\mu_{Fe} = 2.829(\chi^M T)^{1/2}/3^{1/2}$ at various temperatures are given.

plex, which are to be compared with those of the coupled systems below. The moment of 5.13 μ_B is close to those few that have been determined for other $[Fe(SR)_4]^{2-}$ species[35,36] and is otherwise typical of tetrahedral Fe(II).

In treatment of the coupled systems which follow, a phenomenological description of the magnetic interactions has been sought. It is assumed that the degeneracy of the ^5E ground state of the tetrahedral Fe(II) has been lifted by local distortions, affording an orbital singlet. This is the case for several $[Fe(SR)_4]^{2-}$ complexes.[35,36] Mössbauer spectroscopy indicates a d_{z^2} ground state with the first excited state near 1000 cm^{-1}, and ab initio calculations gave about 1400 cm^{-1} for this same gap.[37] The starting point is the usual Heisenberg Hamiltonian (eq 7), summed over three or four Fe(II) centers, and having the eigenvalues of eq 8. Each value of the total spin S corresponds to one energy

$$H = -J\sum_{i<j=1}^{3,4} \vec{S}_i\cdot\vec{S}_j \qquad (7)$$

$$E(S) = (-J/2)[S(S+1)] \qquad (8)$$

level with degeneracy n_S. The molar magnetic susceptibility is given by eq 9, in which allowance has been made for a Curie paramagnetic impurity from an $S = 2$ species (mol fraction ρ).

$$\chi^M = \frac{g^2\beta^2N}{3kT}\frac{\sum_S n_S(2S+1)S(S+1)e^{-E(S)/kT}}{\sum_S n_S(2S+1)e^{-E(S)/kT}}(1-\rho) + \rho\frac{2g^2\beta^2N}{kT} \qquad (9)$$

Inasmuch as all complexes have a diamagnetic ground state, the impurity contribution is most significant at the lower temperatures.

(b) $(Et_4N)_3[Fe_3(SPh)_3Cl_6]$. The temperature dependence of the molar magnetic susceptibility, reported in Figure 6, shows a well-developed maximum at 15 K followed by decreasing susceptibility with increasing temperature. Near 1.8 K the susceptibility passes through a minimum and then rises, owing to an impurity. Magnetic moments per Fe atom, μ_{Fe}, calculated from the Curie law (eq 6, $\alpha = 0$), are strongly depressed below that of $[Fe(SEt)_4]^{2-}$. The behavior overall is characteristic of an antiferromagnetically coupled system, with a Curie-like magnetic impurity detectable only at the lowest temperatures. If Fe(II) atoms 1, 2, and 3 = 2′ (Figure 2) are taken to define an equilateral triangle, then the magnetic coupling constants $J_{12} = J_{23} = J_{13} = J$ in the Hamiltonian eq 7 and local spins $S_1 = S_2 = S_3 = 2$, as for $[Fe(SEt)_4]^{2-}$. Expanding eq 7 gives

$$H = (-J/2)[(\vec{S}_1 + \vec{S}_2 + \vec{S}_3)^2 - \vec{S}_1^2 - \vec{S}_2^2 - \vec{S}_3^2] \qquad (10)$$

the eigenvalues of which are given by eq 8 from which the constant term $3JS_1(S_1+1)/2$ has been omitted. The energy level scheme for the idealized D_{3h} structure of $[Fe_3(SPh)_3Cl_6]^{3-}$ is plotted in Figure 7. Attempts to fit the data to eq 9 were not entirely satisfactory. The best results (not shown) were obtained with $J = -23.0$ cm^{-1}, $g = 2.214$, and $\rho = 0.04$. The fit at ≥45 K was excellent ($R = 2.8 \times 10^{-6}$), but at ~10–40 K the calculated χ^M/T curve fell substantially below the experimental points.

The actual C_2 symmetry of $[Fe_3(SPh)_3Cl_6]^{3-}$ requires two coupling constants, $J_{12} = J_{13} = J$ and $J_{23} = J'$. In this case the appropriate Hamiltonian is

$$H = -J(\vec{S}_1\cdot\vec{S}_2 + \vec{S}_1\cdot\vec{S}_3) - J'(\vec{S}_2\cdot\vec{S}_3) \qquad (11)$$

from which

$$H = (-J/2)[(\vec{S}_1 + \vec{S}_2 + \vec{S}_3)^2 - \vec{S}_1^2 - (\vec{S}_2 + \vec{S}_3)^2] - (J'/2)[(\vec{S}_2 + \vec{S}_3)^2 - \vec{S}_2^2 - \vec{S}_3^2] \qquad (12)$$

The eigenvalues are given by eq 13 where $S' = 0, 1, 2, 3, 4$ and $|S'-2| < S < (S'+2)$. The S' values correspond to coupling of local spins S_1 and S_2. S' is then coupled to S_3 to give the total

$$E(S,S') = (-J/2)[S(S+1) - S'(S'+1)] - (J'/2)[S'(S'+1)] \qquad (13)$$

$S = 0$ (1), 1 (3), 2 (5), 3 (4), 4 (3), 5 (2), 6 (1); degeneracies are given in parentheses. The energy levels $E(S,S')$ are shown in Figure 7. The rapidly decreasing χ^M values at low temperatures in Figure 6 are consistent with the singlet ground state (0,2). For this case the magnetic susceptibility is given by a modified form of eq 9, containing the energies $E(S,S')$ and summed over S,S'. Parameters of the two best fits, which are essentially equally good, are given in Table IX. Impurity corrections are <1 mol % of total iron, and g values are close to that of $[Fe(SEt)_4]^{2-}$. The only important difference between the two fits is the order of J and J', which cannot be settled from the results at hand and affects the fit noticeably only in the narrow region around the maximum

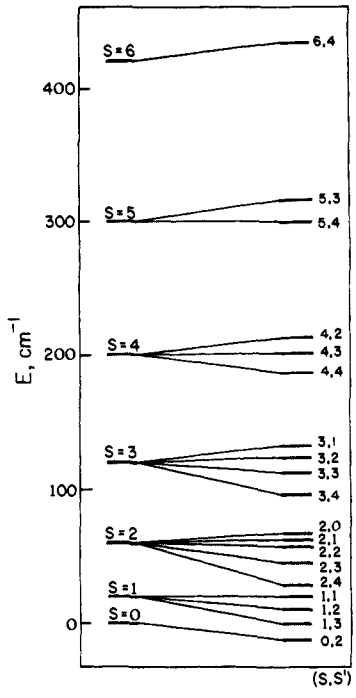

Figure 7. Energy levels for three antiferromagnetically coupled Fe(II) atoms with $J = J_{12} = J_{13} = J_{23} = -20$ cm^{-1} (left) and $J_{12} = J_{13} = -22.5$ cm^{-1} and $J_{23} = -18.7$ cm^{-1} (right).

(35) Lane, R. W.; Ibers, J. A.; Frankel, R. B.; Papaefthymiou, G. C.; Holm, R. H. *J. Am. Chem. Soc.* **1977**, *99*, 84.
(36) Coucouvanis, D.; Swenson, D.; Baenziger, N. C.; Murphy, C.; Holah, D. G.; Sfarnas, N.; Simopoulos, A.; Kostikas, A. *J. Am. Chem. Soc.* **1981**, *103*, 3350.
(37) Bair, R. A.; Goddard, W. A., III *J. Am. Chem. Soc.* **1978**, *100*, 5669.

Table IX. Magnetic Properties of $[Fe_3(SPh)_3Cl_6]^{3-}$ and $[Fe_4(SR)_{10}]^{2-}$ (R = Et, *p*-tol)

complex	mean Fe-(μ_2S), Å	θ, deg	$-J$, cm^{-1}	$-J'$, cm^{-1}	$-J''$, cm^{-1}	g	$\rho \times 10^3$	$R \times 10^4$ [a]
$[Fe_3(SPh)_3Cl_6]^{3-}$	2.356 (8)[b]	2 at 138.9	19.3	23.3		2.136	8.0	8.7
		1 at 142.2	22.5	18.7		2.154	8.0	6.6
$[Fe_4(SEt)_{10}]^{2-}$	2.354 (9)[c,e]	4 at 110.2-111.4	48.2	48.2	48.2	2.176	12	16.0
		2 at 112.8-113.2	65.6	51.2	65.6	2.411	11	7.0
			44.0	32.5	62.9	2.117	14	5.5[f]
$[Fe_4(S\text{-}p\text{-}tol)_{10}]^{2-}$	2.368 (14)[c,d]	4 at 112.5-115.8[d]	34.2	34.2	34.2	1.952	18	16.0
		2 at 108.9-109.7[d]	46.9	36.1	46.9	2.151	11	2.5
			42.5	32.2	46.1	2.085	11	2.2[f]

[a] $R = \sum(\chi^M_{expt} - \chi^M_{calcd})^2/(\chi^M_{expt})^2$. [b] Mean of 3 values. [c] Mean of 12 values. [d] Data for $[Fe_4(SPh)_{10}]^{2-}$ as its Me_4N^+ salt.[3] [e] Reference 6. [f] Parameter sets used in the plots in Figure 8.

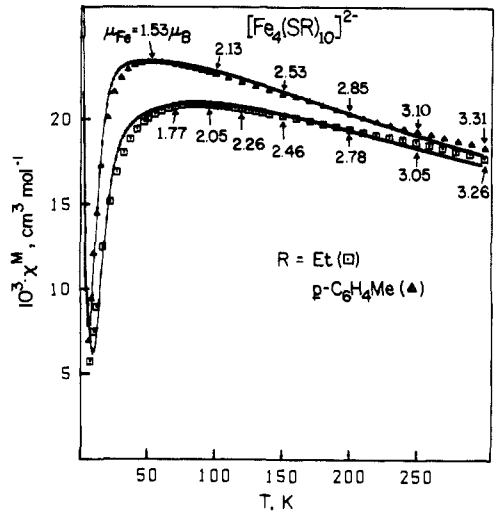

Figure 8. Temperature dependencies of the molar magnetic susceptibilities of $(Me_4N)_2[Fe_4(SEt)_{10}]$ ($J = -44.0$, $J' = -32.5$, $J'' = -62.9$ cm^{-1}) and $(n\text{-}Bu_4N)_2[Fe_4(S\text{-}p\text{-}tol)_{10}]$ ($J = -42.5$, $J' = -32.2$, $J'' = -46.1$ cm^{-1}). The solid lines are theoretical fits to the data with use of the indicated J values and associated parameters in Table IX. Values of $\mu_{Fe} = \mu/2$ at various temperatures are given.

χ^M value. Inclusion of distortion of the complex to its actual twofold symmetry, with attendant splitting of low-lying states according to S', markedly improves the fit in this region compared to that for threefold symmetry. This is the case even though differences in structural features associated with the inequivalence of Fe(1) and Fe(2,2') are relatively small. Above ~45 K the effect of the lower symmetry is imperceptible, and the calculated χ^M/T curves merge with that for a single J value of -23.0 cm^{-1} and the foregoing g value.

(c) $[Fe_4(SR)_{10}]^{2-}$. The temperature dependencies of the molar magnetic susceptibilities of $(Me_4N)_2[Fe_4(SEt)_{10}]$ and $(n\text{-}Bu_4N)_2[Fe_4(S\text{-}p\text{-}tol)_{10}]$, provided in Figure 8, reveal maxima near 85 and 55 K, respectively. This result immediately points to weaker antiferromagnetic coupling in $[Fe_4(S\text{-}p\text{-}tol)_{10}]^{2-}$. In the first stage of analysis, the $Fe_4(\mu_2\text{-}S)_6$ cage portions of $[Fe_4(SR)_{10}]^{2-}$ were idealized to T_d symmetry, and fits of the magnetic data with a single J value were investigated by use of eq 9. In this case S = 0 (5), 1 (12), 2 (16), 3 (17), 4 (15), 5 (10), 6 (6), 7 (3), and 8 (1), with the indicated degeneracies n_S. The parameter sets in Table IX, with $J = -48.2$ cm^{-1} for $[Fe_4(SEt)_{10}]^{2-}$ and $J = -34.2$ cm^{-1} for $[Fe_4(S\text{-}p\text{-}tol)_{10}]^{2-}$, gave fairly good fits (not shown) at temperatures near and above the maxima but were less satisfactory at the lower temperatures. Inasmuch as the cages are in fact appreciably distorted from T_d symmetry,[3,6] these J values can be considered rough means of the different actual J values.

Improved fits of the magnetic data require more than one J value and recognition of different coupling symmetries in the $Fe_4(\mu_2\text{-}S)_6$ cage. For a two-J fit analytical solutions of the eigenvalues can be found with Hamiltonians corresponding to C_s, C_{2v}, C_{3v}, and D_{2d} symmetry, and for a three-J fit in C_s and C_{2v} symmetry. The detailed structures of $[Fe_4(SPh)_{10}]^{2-}$[3] and $[Fe_4(SEt)_{10}]^{2-}$[6] reveal that bridge angles tend to divide into the 4 + 2 sets in Table IX. On this basis $[Fe_4(SEt)_{10}]^{2-}$ has C_s cage symmetry in the angles θ, suggesting this as a coupling symmetry under which to investigate fits. The appropriate Hamiltonian is

$$H = -J(\vec{S}_1\cdot\vec{S}_2 + \vec{S}_1\cdot\vec{S}_3 + \vec{S}_2\cdot\vec{S}_3 + \vec{S}_3\cdot\vec{S}_4) - J'(\vec{S}_1\cdot\vec{S}_4 + \vec{S}_2\cdot\vec{S}_4) \quad (14)$$

for which the eigenvalues are

$$E(S,S',S'') = (-J/2)[S(S+1) - S'(S'+1)] - (J/2)[S''(S''+1)] - (J'/2)[S'(S'+1) - S''(S''+1)] \quad (15)$$

with

$$0 \le S'' \le 4$$

$$|S'' - 2| \le S' \le (S'' + 2)$$

$$|S' - 2| \le S \le (S' + 2)$$

The treatment is an extension of the 3Fe(II) case with two J values. The magnetic susceptibility is given by eq 9 with substitution by $E(S,S',S'')$ and summation over S,S',S''. Fits for both compounds are markedly improved; best-fit parameters are listed in Table IX. Inasmuch as not all Fe(II) cage complexes (e.g., $[Fe_4(SCH_2Ph)_6Br_4]^{2-}$) exhibit C_s cage angle symmetry, three-J fits were investigated. A detailed treatment, which is a lengthy extension of the foregoing analyses, is omitted and the results are summarized. Fits to the data of both $[Fe_4(SEt)_{10}]^{2-}$ and $[Fe_4(S\text{-}p\text{-}tol)_{10}]^{2-}$ in C_s symmetry ($2J + J' + 3J''$) are somewhat improved over two-J treatments (Table IX). However, even at this level of parametrization the theoretical curves in Figure 8 do not coincide with experimental data over the entire temperature interval. Much inferior fits were obtained for $[Fe_4(S\text{-}p\text{-}tol)_{10}]^{2-}$, whose detailed structure is unknown, using other models including D_{2d} ($4J + 2J'$) and C_{2v} ($4J + J' + J''$). The lack of any cage symmetry contributes to the difficulty in fitting the magnetic data.

The magnetic susceptibility results and analyses demonstrate that $[Fe_3(SPh)_3Cl_6]^{3-}$ and $[Fe_4(SR)_{10}]^{2-}$ (R = Et, *p*-tol) are molecular antiferromagnets with singlet ground states. This property accounts for the well-resolved, contact-shifted ^{1}H NMR spectra of $[Fe_4(SR)_{10}]^{2-}$[3,6] and $[Fe_3(SR)_3X_6]^{3-}$ considered in the following section. Values of $|J|$ tend to increase as the bridge angle decreases in going from $[Fe_3(SPh)_3Cl_6]^{3-}$ to $[Fe_4(SR)_{10}]^{2-}$, regardless of the parametrization of the fits. Within a given species, where there is a better basis for comparison, it is not possible to prove a correlation between θ and J values. Earlier results for thiolate complexes containing $Fe_2(\mu_2\text{-}S)_2$ units,[38] together with the present findings, suggest that antiferromagnetic interactions are intrinsic to $Fe^{II}\text{-}(\mu_2\text{-}S)\text{-}Fe^{II}$ bridges. Further comparison with the complexes examined here is inappropriate owing to differences in coordination geometry and attendant d-orbital splittings and a contribution to exchange from direct Fe-Fe interaction.[38]

Solution Behavior. The unusual nature of the cyclic $[Fe_3(SR)_3X_6]^{3-}$ structure in the crystalline state raises the question of the stability of $Fe_3(SR)_3$ rings in solution, a matter examined

(38) Ginsberg, A. P.; Lines, M. E.; Karlin, K. D.; Lippard, S. J.; DiSalvo, F. J. *J. Am. Chem. Soc.* **1976**, *98*, 6958.

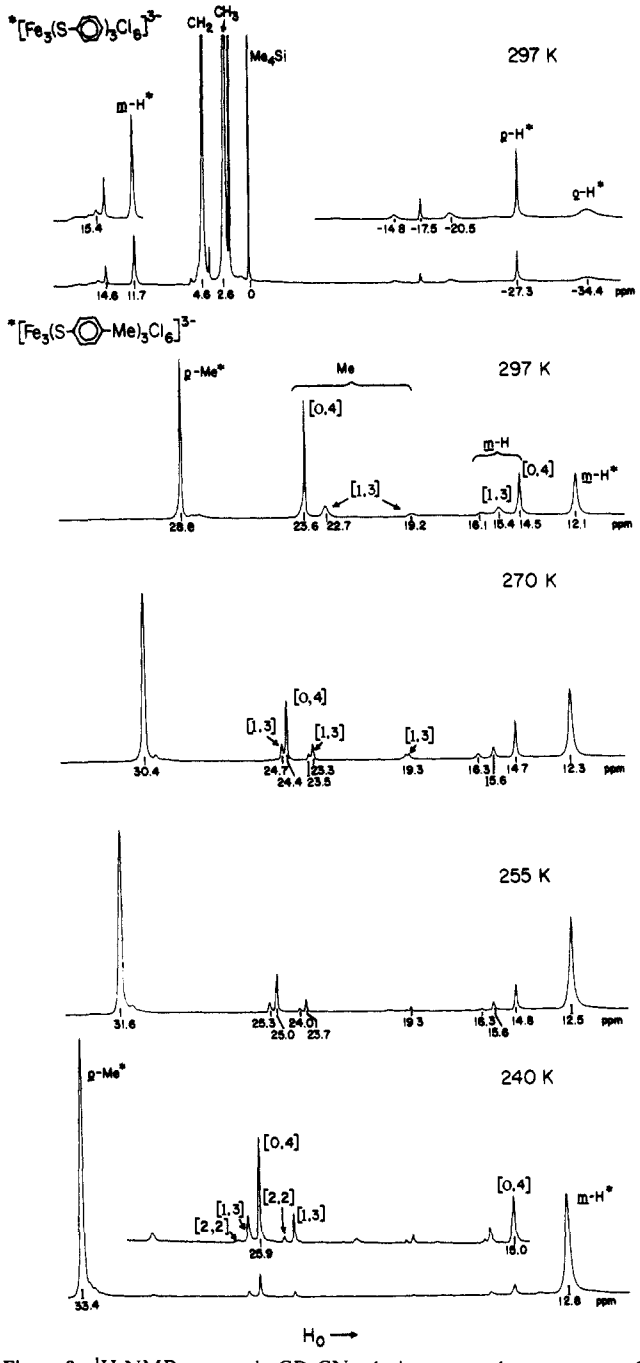

Figure 9. ^1H NMR spectra in CD_3CN solutions: complete spectrum of $[Fe_3(SPh)_3Cl_6]^{3-}$ and the downfield region of the spectrum of $[Fe_3(S\text{-}p\text{-}tol)_3Cl_6]^{3-}$ ([Fe] ~ 60 mM) at various temperatures. Signal assignments are indicated; bracketed designations of species are defined in Figure 10.

by ^1H NMR. The major signals of the 297 K spectrum of an acetonitrile solution prepared from $(Et_4N)_3[Fe_3(SPh)_3Cl_6]$, shown in Figure 9, are readily assigned. At 243 K (not shown), the relative intensities of the signals at 11.7, −27.3, and −34.4 ppm (297 K) are unchanged, indicating that these signals belong to a single species. The absence of the −27.3-ppm resonance in the $[Fe_3(S\text{-}p\text{-}tol)_3Cl_6]^{3-}$ spectrum at 297 K and relative intensities and line widths leads to the indicated assignments for $[Fe_3(SPh)_3Cl_6]^{3-}$. Similar considerations afford the assignments for $[Fe_3(S\text{-}p\text{-}tol)_3Cl_6]^{3-}$, whose well-resolved downfield spectra at various temperatures are included in Figure 9. The alternation in sign of the *o*-, *m*-, and *p*-H and of *p*-H/*p*-Me isotropic shifts and increases of these shifts with decreasing temperature[39] are consistent with the presence of contact interactions, also a property

(39) $(\Delta H/H_0)_{iso} = (\Delta H/H_0)_{obs} - (\Delta H/H_0)_{dia}$. Isotropic shifts at 297 (243) K: *o*-H, +41.6 (+47.2); *m*-H, −4.5 (−5.0); *p*-H, +34.5 (+39.4) ppm.

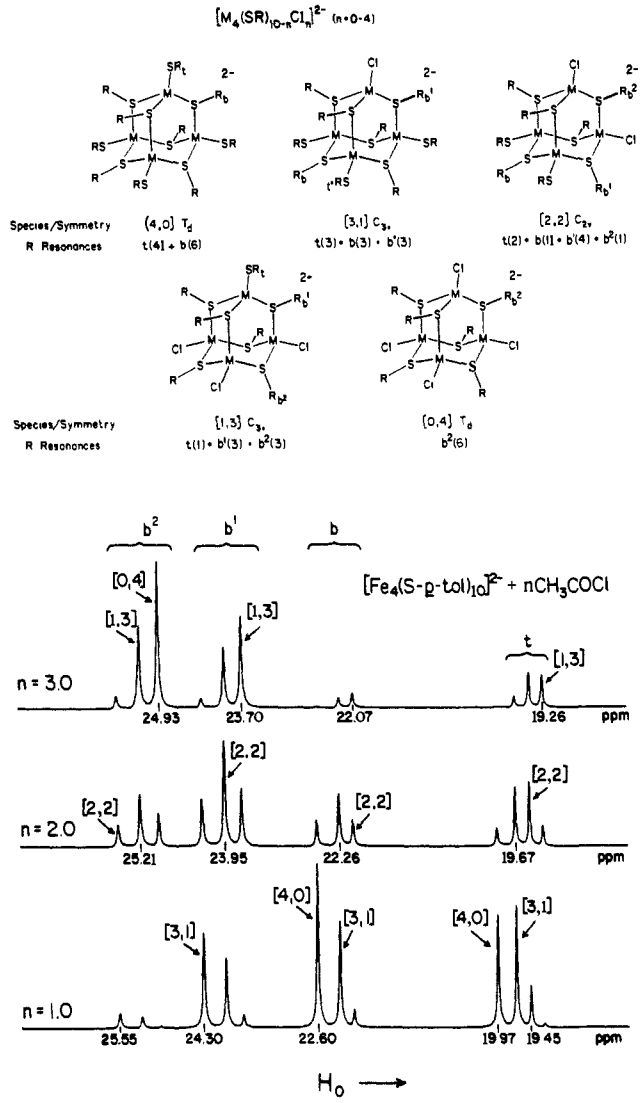

Figure 10. Upper: schematic representations of cage structures in the series $[M_4(SR)_{10-n}Cl_n]^{2-}$ (n = 0–4). The type and number of inequivalent R groups under the indicated idealized symmetries are shown (b = bridging, t = terminal); only one R group of a given type is labeled. Lower: *p*-Me ^1H NMR spectra (~270 K) of $[Fe_4(S\text{-}p\text{-}tol)_{(0-n}Cl_n]^{2-}$, generated by the reaction of $[Fe_4(S\text{-}p\text{-}tol)_{10}]^{2-}$ and n = 1–3 equiv of CH_3COCl in CD_3CN. Signal assignments are indicated.

of $[Fe(SPh)_4]^{2-}$[2] and $[Fe_4(SPh)_{10}]^{2-}$.[3] The second feature requires an increase in susceptibility with decreasing temperature at ~ 240–300 K, which is observed in the solid state (Figure 6). While the major signals in the spectra of Figure 9 arise from $[Fe_3(SR)_3Cl_6]^{3-}$, there remain resonances of significant intensities in the upfield and downfield regions. These have been identified by using the information in Figure 10 and reaction systems with R = *p*-tol because of the superior resolution of the *p*-Me signal.

Reaction 16 with 1–4 equiv of acetyl chloride results in the replacement of terminal ligands only. By analogy with the $[Fe_4S_4(SR)_4]^{2-}/CH_3COCl$[40] and related systems[19] containing remote thiolate ligands on a common core structure, this reaction

$$[Fe_4(SR)_{10}]^{2-} + nCH_3COCl \rightarrow [Fe_4(\mu_2\text{-}SR)_6(SR)_{4-n}Cl_n]^{2-} + nCH_3COSR \quad (16)$$

should generate a nearly statistical distribution of products [4 − *n*,*n*]. Their structures and NMR signal multiplicities are given in Figure 10 together with spectra of n = 1–3 systems, which cover the methyl region and were recorded at ~270 K to improve signal resolution. All spectral features can be definitely assigned on the basis of growth and decay of intensities with increasing n and

(40) Johnson, R. W.; Holm, R. H. *J. Am. Chem. Soc.* **1978**, *100*, 5338.

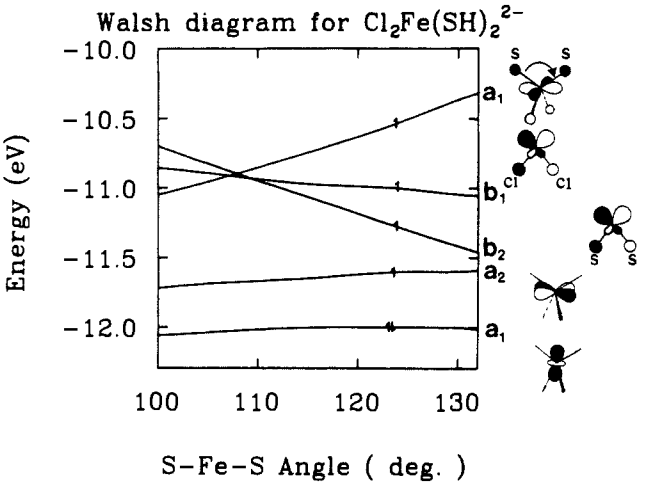

Figure 11. Dependence of the energies of d-type orbitals on the S-Fe-S angle in tetrahedral (C_{2v}) $[Fe(SH)_2Cl_2]^{2-}$. Schematic representations of the metal and ligand contributions to the orbitals are presented.

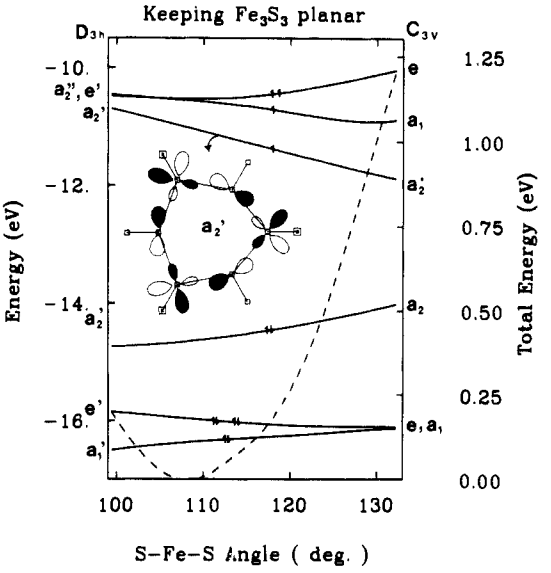

Figure 12. Orbital energy changes accompanying the distortion of $[Fe_3(SH)_3Cl_6]^{3-}$ from D_{3h} to C_{3v} symmetry as the S-Fe-S angle is varied and H atoms are on the same side of the Fe_3S_3 plane. The dashed line represents the total energy change scaled to the right-hand ordinate axis with the lowest energy value arbitrarily taken as zero. A schematic representation of the Fe-S antibonding orbital a_2', which correlates with a_2^* under C_{3v} symmetry, is given.

relative intensities of signals. In the $n = 1$ system, the dominant species are [4,0] and [3,1] with two and three signals, respectively. At $n = 2$ the maximum of 13 signals arising from the five possible species with $n = 0$–4 are observed.[41] In the $n = 3$ system [1,3] and [0,4] are the main species. For these systems there are six equilibria and three independent equilibrium quotients, chosen here for reactions 17–19. Equilibrium constants evaluated from signal intensities agree well with statistical values (parentheses).

$$[4,0] + [2,2] \rightleftharpoons 2[3,1] \qquad K = 2.6\ (2.67) \qquad (17)$$

$$[3,1] + [1,3] \rightleftharpoons 2[2,2] \qquad K = 2.1\ (2.25) \qquad (18)$$

$$[2,2] + [0,4] \rightleftharpoons 2[1,3] \qquad K = 2.6\ (2.67) \qquad (19)$$

Comparison of the 270 K spectrum in Figure 9 with those in Figure 10, especially that for $n = 3$, leads to identification of all minority signals with the indicated species. Of these, [0,4] is formed in the largest amount followed by a much smaller amount of [1,3] and a barely detectable concentration of [2,2]. Given the predominance of [0,4] among the minority products, the *main* equilibrium in solution appears to be reaction 20. This is shifted

$$2[Fe_3(SR)_3Cl_6]^{3-} \rightleftharpoons [Fe_4(SR)_6Cl_4]^{2-} + 2[FeCl_4]^{2-} \qquad (20)$$

to the left with decreasing temperature. The two other trinuclear complexes behave similarly. For example, at 297 K the *o*-Me (37.9), *m*-H (27.0), and *p*-H (−38.8 ppm) resonances of $[Fe_3(SMe_2Ph)_3Cl_6]^{3-}$ are accompanied by a set of minority signals. At 240 K the cyclic trimer signals occur at 47.2, 24.9, and −46.3 ppm, and the minority signals are barely detectable.

Reaction 20 was further examined by means of a CD_3CN solution initially containing a 2:1 ratio of $(Et_4N)_2[FeCl_4]$ and $(Ph_4P)_2[Fe_4(S\text{-}p\text{-}tol)_6Cl_4]$[27] at a total Fe concentration of 49 mM. The NMR spectrum of this solution at 297 K (not shown) reveals the characteristic signals of $[Fe_3(S\text{-}p\text{-}tol)_3Cl_6]^{3-}$ at this temperature, a relatively smaller amount of starting complex [0,4] than in the system of Figure 9, and a minor broad peak of unknown origin at 17.5 ppm. The species [1,3] and [2,2] were not detected. In this approach and that in Figure 9 to reaction 20 the cation content is not constant inasmuch as we were unable to isolate the Et_4N^+ salt of $[Fe_4(S\text{-}p\text{-}tol)_6Cl_4]^{2-}$. Cations do interact with $[Fe_3(SR)_3X_6]^{3-}$ and may affect the position of equilibrium. The resonances of Et_4N^+, which normally occur at 1.2 and 3.2 ppm in CD_3CN, are shifted downfield to 2.6 and 4.6 ppm in the presence of $[Fe_3(SPh)_3Cl_6]^{3-}$ (Figure 9). Further, these shifts vary with concentration and temperature in a manner indicative of ion pairing, by which the dipolar paramagnetic shifts of the cation are developed. These interactions are also seen in the solid state where Et_4N^+ ions are located above each phenyl ring of $[Fe_3(SPh)_3X_6]^{3-}$ (X = Cl^-, Br^-). Equilibrium 20 has been approached from both directions and, cation differences notwithstanding, it is clear that the cyclic trimer is the dominant solution species and that its concentration increases with decreasing temperature. The presence of $[FeCl_4]^{2-}$ has not been directly proven; it is the simplest non-thiolate Fe(II) complex to satisfy the material balance of the reaction. We have been unable to identify the origin of the very slight amounts of [1,3] and [2,2] formed by dissolution of the compounds $(Et_4N)_3[Fe_3(SR)_3X_6]$ in acetonitrile.

Analysis of Fe_3S_3 Ring Geometry. Maintenance of the cyclic structure of $[Fe_3(SR)_3X_6]^{3-}$ with different phenyl group orientations and sizes of X ligands and in acetonitrile solution (vide infra) indicates a ring of stability sufficient to warrant an analysis of its metric and conformational features. Here we investigate the unusual geometric aspects of the Fe_3S_3 ring in terms of several closely related questions. Why do these rings assume a planar instead of a nonplanar arrangement, specifically, the chair conformation of the $Fe_3(\mu_2\text{-}S)_3$ rings present in $[Fe_4(SR)_{10}]^{2-}$ and $[Fe_4(SR)_6X_4]^{2-}$? Why are the Fe_2SC fragments planar instead of pyramidal, and why are the Fe–S–Fe angles abnormally large (~140°) compared to those in the foregoing cage complexes (~110°)? These matters have been addressed by calculations at the extended Hückel level of approximation.[42] Central to our approach are the works of Summerville and Hoffmann[43] and Shaik et al.,[44] who investigated theoretically the geometrical preferences of M_2L_6 and M_2L_{10} dimers, respectively. Considered first is the fragment species $[Fe(SH)_2Cl_2]^{2-}$ of the hypothetical trimer $[Fe_3(SH)_3Cl_6]^{3-}$, utilized for calculational simplicity.

$[Fe(SH)_2Cl_2]^{2-}$ is derived from the T_d complex $[FeCl_4]^{2-}$, has C_{2v} symmetry and four π-donor ligands, and was idealized from average dimensions of $[Fe_3(SPh)_3Cl_6]^{3-}$ as follows: the Cl–Fe–Cl angle was fixed at 112.75°, Fe–Cl and Fe–S bond distances were set at 2.274 and 2.356 Å, respectively, and H atoms were placed along the S–C(Ph) vector with a S–H distance of 1.34 Å. In this

(41) At $n = 2$ the statistical mol fractions are [4,0] = [0,4] = 0.063, [3,1] = [1,3] = 0.250, and [2,2] = 0.375.

(42) Calculation of H_{ij}: Ammeter, J. H.; Bürgi, H.-B.; Thibeault, J. C.; Hoffmann, R. *J. Am. Chem. Soc.* **1978**, *100*, 3686. S parameters: Burdett, J. K. *Molecular Shapes*; Wiley-Interscience: New York, 1980; p 28. Other parameters are given elsewhere.[43]

(43) Summerville, R. H.; Hoffmann, R. *J. Am. Chem. Soc.* **1976**, *98*, 7240.

(44) Shaik, S.; Hoffmann, R.; Fisel, C. R.; Summerville, R. H. *J. Am. Chem. Soc.* **1980**, *102*, 4555.

symmetry the d-orbitals transform as $2a_1 + a_2 + b_1 + b_2$. The purpose of the calculations on the monomer was to investigate the S–Fe–S angle preference in a coordination environment similar to that in $[Fe_3(SPh)_3Cl_6]^{3-}$, where the mean angle is 100°. In a planar Fe_3S_3 ring of D_{3h} symmetry, a S–Fe–S angle of 100° enforces a Fe–S–Fe angle of 140°. The former angle was varied in the range 100–132° at constant Cl–Fe–Cl angle; the behavior of the d-type orbitals is shown in the Walsh diagram of Figure 11, in which the ground state d-electron configuration is indicated. The a_1 orbital, corresponding to $d_{x^2-y^2}$ in the planar limit, becomes destabilized as σ-antibonding effects increase when the angle is opened up. This behavior favors the observed angle of 100°. Conversely, the b_2 orbital is stabilized at the larger angles as sulfur atoms move toward the nodal surface of the d/p hybrid orbital. Energies of the remaining orbitals are largely unaffected by changes in the S–Fe–S angle. The total energy of $[Fe(SH)_2Cl_2]^{2-}$ is constant over the range 100–120°, but increases at larger angles and at 132° amounts to a 0.3-eV destabilization compared to the constant range. If the window of acceptable angles is this range, the complementary interval of Fe–S–Fe angles is 140–120° for a planar ring. While these results do not single out the observed angles, they do suggest that the intrinsically preferred Fe–S–Fe angle ought to be at least ~120°. This corresponds to nearly planar thiolate stereochemistry in a bridged arrangement, according to the θ/ϕ criterion of Dance et al.[15]

Calculations were next performed for $[Fe_3(SH)_3Cl_6]^{3-}$ with bond lengths as in $[Fe(SH)_2Cl_2]^{2-}$. In the first stage D_{3h} symmetry was imposed, the bond distances in $[Fe(SH)_2Cl_2]^{2-}$ were retained, and the S–Fe–S and Fe–S–Fe angles were varied over the ranges 99.5–132° and 140.5–108°, respectively. Although ring planarity was maintained, the SH groups were required to respond to the angular changes by bending out of the plane by an angle ϕ, in accordance with the empirical θ/ϕ curve of Dance et al.[15] The bending of these groups can result in structures of C_{2v} or C_{3v} symmetry. Results of calculations for both cases are similar. Consequently, only the C_{3v} case **7**, in which all H atoms are on the same side of the ring, will be considered. Because the Fe(II) atoms in $[Fe_3(SPh)_3Cl_6]^{3-}$ are only weakly antiferromagnetically coupled, each such atom retains the spin-quintet description of the monomer. The behavior of those orbitals *most affected* by the angular deformations is shown in Figure 12.

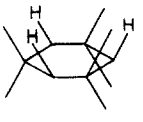

7

The important orbitals fall into three groups.[45] Those between −10 and −12 eV are singly occupied and are most readily described by reference to the orbitals of the monomer (Figure 12). The e set near −10 eV, which are the highest occupied orbitals of the C_{3v} structure, is derived from the $d_{x^2-y^2}$-type a_1 orbital and consequently destabilizes with increasing S–Fe–S angle. The a_2'' orbital, the HOMO of the D_{3h} structure, is a descendent of the monomer b_1 orbital, correlates with a_1 under C_{3v} symmetry, and has antibonding Fe–Cl $\sigma + \pi$ character. The a_2^* orbital, schematically depicted in Figure 12, is derived from monomer orbital b_2. It is stabilized at large S–Fe–S angles because antibonding overlap decreases as sulfur orbitals approach the nodal surface of the d/p hybrids at the Fe atoms. The a_2 orbital at −14 to −15 eV is the σ-bonding complement of a_2^*; consequently, it is destabilized as the angle is opened. Although the slope of a_2^* is steeper than that of a_2, the latter is bonding and doubly occupied and thus contributes to the instability of the larger angles. The low-lying MOs near −16 eV are composed of S–H orbitals. At an angle of 100° the S···S distance is 3.6 Å and interactions among sulfur atoms spread e′ and a_1' apart. This spread is diminished as the S···S distance increases with increasing angle. The minimum energy structure, under the constraint of D_{3h} symmetry, has an S–Fe–S angle of about 108°. This value is in the acceptable range of monomer angles and is in reasonable agreement with the experimental value of 100°.

(45) $[Fe_3(SH)_3Cl_6]^{3-}$ has 66 MOs, of which 15 are unoccupied. The highest 15 occupied orbitals (ca. −10 to −12.5 eV) are significantly d in character. Below these lie 36 filled ligand-based MOs at ca. −13.5 to −31 eV. The HOMO–LUMO gap is ~10 eV. Because of the large number of MOs, only those whose energies are most affected by S–Fe–S angle changes are included in Figure 13.

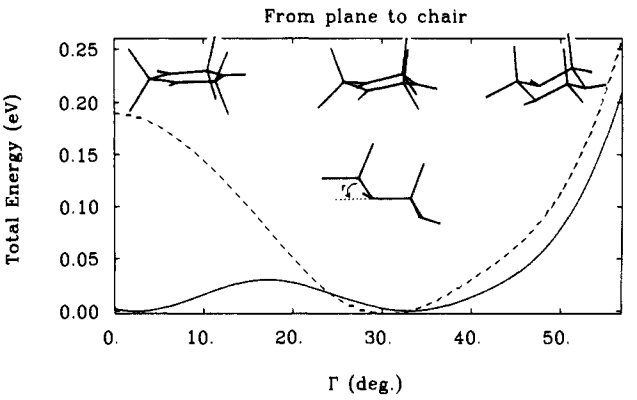

Figure 13. Energy changes as $[Fe_3(SH)_3Cl_6]^{3-}$ is altered from a planar to a chair conformation. The solid line represents the total energy, and the dashed line is the result of subtracting the contribution of d-electrons from the total energy. For both curves the zero of energy is arbitrary. The distortion coordinate Γ, which is the dihedral angle of inclination of the FeS_2 to the Fe_2S_2 plane, is illustrated. Snapshots of conformations along the distortion coordinate are provided.

In the final set of calculations the planar ring structure was altered to a chair conformation, such as is found in $[Fe_4(SEt)_{10}]^{2-}$.[6] This was accomplished by keeping the S···S distances fixed and increasingly rocking the $FeCl_2$ units up relative to the S_3 plane. Hydrogen atoms were placed by means of the θ/ϕ correlation.[15] Presented in Figure 13 is a plot of total energy as a function of the distortion coordinate Γ, the dihedral angle between the FeS_2 and Fe_2S_2 planes. Depictions of ring conformations along this coordinate are provided. The total energy is nearly flat at $\Gamma \cong$ 0–40° and then increases rapidly at larger angles. By this criterion the planar ring is 0.21 eV more stable than the perfect chair form (Γ = 56.8°). When the contribution of d-electrons is subtracted, a conformation intermediate between plane and chair is predicted.

The following qualitative conclusions emerge from the MO analysis. The stereochemical preference of the S–Fe–S angle in the monomer $[Fe(SH)_2Cl_2]^{2-}$ is broad (~100–120°). Adoption of the lowest value of this angle in a planar (D_{3h}) ring enforces an unusually large Fe–S–Fe angle of ~140°, an arrangement observed in three complexes. The theoretically predicted S–Fe–S angle is 108° (Figure 12), in reasonable agreement with experiment considering the simplicity of the model. Values of this angle in excess of ~120° should afford ring structures of considerably less relative stability. Planar stereochemistry at sulfur is clearly associated with the markedly open Fe–S–Fe angles, a situation that may be roughly likened to a transition state for the (usually facile) inversion of coordinated thiolate in M_2SR groups.[46] There is a small preference (~5 kcal/mol) for a planar or nonplanar ($\Gamma \cong$ 0–40°) vs. the limiting chair conformation. The destabilization of the chair form reflects unfavorable core effects, including transannular nonbonded repulsions. The energetics of these repulsions are parameter-dependent at the extended Hückel level, but the decrease in, e.g., Cl···Cl distances from 6.62 Å in the planar to 3.87 Å in the chair conformation, makes evident their importance in stabilizing a planar ring structure. (Such distances are even more destabilizing in alternative nonplanar arrangements.) Given the larger van der Waals radius of Br compared to Cl, transannular contacts especially favor the planar structure in the case of $[Fe_3(SPh)_3Br_6]^{3-}$. Furthermore, ligand–ligand repulsions are certainly greater for the real $[Fe_3(SR)_3Cl_6]^{3-}$ complexes (R = aryl) than for $[Fe_3(SH)_3Cl_6]^{3-}$. In a similar context others[43,44,47] have pointed out the importance of ligand–

(46) Abel, E. W.; Bhargava, S. K.; Orrell, K. G. *Prog. Inorg. Chem.* **1984**, *32*, 1.

Table X. Magnetic Moments of Fe(II) Complexes in the Solution and Solid States at Selected Temperatures

$(Et_4N)_3[Fe_3(SPh)_3Cl_6]$				$(n\text{-}Bu_4N)_2[Fe_4(S\text{-}p\text{-}tol)_{10}]$		$(Me_4N)_2[Fe_4(SEt)_{10}]$	
CD_3CN soln[a]		solid		solid		solid	
T, K	μ_{Fe}[b]	T, K	μ_{Fe}[b]	T, K	μ_{Fe}[c]	T, K	μ_{Fe}[c]
299	4.48	301.8	4.33	300.4	3.31	300.0	3.26
294	4.47	291.8	4.31	290.4	3.28	288.9	3.22
283	4.40	281.6	4.28	280.4	3.23	278.5	3.17
267	4.30	271.6	4.25	270.4	3.19	268.7	3.13
251	4.22	251.5	4.18	250.3	3.10	249.1	3.04
235	4.16	231.4	4.10	230.3	3.00	239.2	3.00

[a] Mean values of two experiments at [Fe] = 17.8 and 27.9 mM. [b] $\mu_{Fe} = 2.829(\chi^{M}_{T})^{1/2}/(3)^{1/2}$. [c] $\mu_{Fe} = 2.829(\chi^{M}_{T})^{1/2}/2$.

ligand repulsions in setting the geometries of bridged complexes.

Ring Conformation in Solution. If, as the three crystal structures and the results of the MO calculations suggest, the Fe_3S_3 rings in $[Fe_3(SR)_3X_6]^{3-}$ have an intrinsic preference for a planar or near-planar conformation, this preference should be expressed in solution. In a weakly coordinating solvent such as acetonitrile, constraints on structure such as are imposed in the crystalline state will be removed. A differentiation between two ring conformations—planar, as found in solid $(Et_4N)_3[Fe_3(SR)_3X_6]$, and chair-type, as in salts of $[Fe_4(SR)_6X_4]^{2-}$ (X = Cl^-, Br^-, RS^-)—can be made on the basis of magnetic properties. As already determined, the cage complexes are more strongly antiferromagnetically coupled than is $[Fe_3(SPh)_3Cl_6]^{3-}$ (Table IX), with the result that μ_{Fe} values of the former are lower at the same temperature. The magnetic moments collected in Table X for the interval 230–300 K illustrate this point. Also included are the moments of $[Fe_3(SPh)_3Cl_6]^{3-}$ in acetonitrile solution. Values in the two phases correspond closely up to about 270 K and are in the 4.1–4.3-μ_B range. Particularly significant is the agreement at 235 K, the lowest temperature of solution measurement. As with the $[Fe_3(S\text{-}p\text{-}tol)_3Cl_6]^{3-}$ system (Figure 9), the solution species is overwhelmingly the cyclic trimer, $[Fe_3(SPh)_3Cl_6]^{3-}$. At 230–250 K the moments of the two cage complexes, 3.0–3.1 μ_B, with their chair-type rings, are much lower. Consequently, *the conformation of the Fe_3S_3 ring of $[Fe_3(SPh)_3Cl_6]^{3-}$, and presumably of other $[Fe_3(SR)_3X_6]^{3-}$ complexes, is planar in acetonitrile solution.* At higher temperatures the solution moments show a somewhat larger departure from the solid-state values, reaching 4.48 μ_B at 299 K. This behavior is consistent with equilibrium 20. Assuming a negligible effect of terminal ligand on cage magnetic coupling, we take $\mu_{Fe} = 3.30\ \mu_B$ for $[Fe_4(S\text{-}p\text{-}tol)_6Cl_4]^{2-}$ (Table X) and 5.40 μ_B for $[FeCl_4]^{2-}$.[48] For the mixture $2[FeCl_4]^{2-}$:$[Fe_4(S\text{-}p\text{-}tol)_6Cl_4]^{2-}$, $\mu_{Fe} = ([2(5.40)^2 + (3.30)^2]/3)^{1/2} = 4.80\ \mu_B$. Therefore, any displacement of equilibrium 20 to the right will cause μ_{Fe} to increase over the value for $[Fe_3(S\text{-}p\text{-}tol)_3Cl_6]^{3-}$ alone.

Summary. The following are the principal findings and conclusions of this investigation.

(1) Systems of equimolar FeX_2 and RS^- in acetonitrile (reaction 5) afford $[Fe_3(SR)_3X_6]^{3-}$ (R = Ph, *p*-tol, 2,6-$Me_2C_6H_3$; X = Cl^-, Br^-), which can be isolated as Et_4N^+ salts. Species of this type apparently complete the set of isolable molecular iron(II) thiolates, other members of the set being $[Fe(SR)_4]^{2-}$, $[Fe_2(SR)_6]^{2-}$, and $[Fe_4(SR)_{10}]^{2-}$. A comparable system with $FeBr_2$ and the alkanethiolate $PhCH_2S^-$ gave the adamantane-like cage complex $[Fe_4(SCH_2Ph)_6Br_4]^{2-}$ rather than the cyclic trimer.

(2) The structure of $[Fe_3(SR)_3X_6]^{3-}$ contains distorted tetrahedral $Fe(SR)_2Cl_2$ units, nearly or exactly planar $Fe_3(\mu_2\text{-}S)_3$ rings, and Fe–S–Fe internal angles of ~140°, the largest observed values for this bridging group. These aspects are independent of X and the orientation of substituent R, which may be coplanar with (Ph) or perpendicular to (2,6-$Me_2C_6H_3$) the central ring.

(3) $[Fe_3(SPh)_3Cl_6]^{3-}$ is antiferromagnetic and is less strongly coupled ($-J$ = 19–22 cm^{-1}) than are $[Fe_4(SEt)_{10}]^{2-}$ ($-J$ = 32–66 cm^{-1}) and $[Fe_4(S\text{-}p\text{-}tol)_{10}]^{2-}$ ($-J$ = 32–47 cm^{-1}), which contain chair-type $Fe_3(\mu_2\text{-}SR)_3$ rings and Fe(II) atoms separated by 3.8–4.0 Å. Satisfactory theoretical fits of the magnetic data have been obtained with two or three J values in the indicated ranges.

(4) Equilibrium 20 in acetonitrile solution has been demonstrated by approaches from both directions and is shifted essentially completely in favor of $[Fe_3(SR)_3X_6]^{3-}$ at $\lesssim$240 K and [Fe] $\gtrsim$ 50 mM.

(5) The indistinguishable magnetic moments μ_{Fe} = 4.1–4.3 of $[Fe_3(SPh)_3Cl_6]^{3-}$ in the solid state and in acetonitrile solution at 235–270 K demonstrate a planar ring conformation in solution, a matter further supported by the lower moments μ_{Fe} = 3.0–3.2 μ_B for $[Fe_4(SR)_{10}]^{2-}$ in the solid state at comparable temperatures.

(6) The collective results of (2) and (5) show that the planar ring structure of $[Fe_3(SR)_3X_6]^{3-}$, at least with the combinations of R and X groups tested, is an intrinsic property, i.e., not determined by crystal packing energetics. This conclusion is consonant with the results of extended Hückel MO calculations, which afford the estimate that the planar conformation is more stable than the chair form by ~0.2 eV (5 kcal/mol). The open Fe–S–Fe angles (~140°) derive largely from the tendency of Fe(II) to stabilize a S–Fe–S angle (110°) near the tetrahedral value, and the planar conformation is stabilized vs. nonplanar structures by lessened transannular nonbonded repulsions.

It remains to be discovered whether analogous complexes $[M_3(SR)_3X_6]^{3-}$ with similar structures can be prepared for other M(II) atoms with tetrahedral stereochemical preference. Variations of reactions 5 and 20 represent starting points for such attempts.

Acknowledgment. This research was supported at Harvard University by NIH Grant 28856 and at the Lawrence Berkeley Laboratory by the Director, Office of Energy Research, Office of Basic Energy Sciences, Chemical Sciences Division of the U.S. Department of Energy under Contract No. DE-AC03-76SF00098. X-ray diffractometers were obtained by NSF Grant CHE 80-06601 and NIH Grant 1 S10 RR02247. We thank D. Wiley and S. Harrison for the use of their diffractometer to collect a Cu radiation data set and D. Freyman for assistance with the data collection. Helpful discussions with D. M. Hoffman, R. Hoffmann, and Y. Apeloig are acknowledged.

Supplementary Material Available: Full sets of observed and calculated magnetic susceptibility data plotted in Figures 6 and 8; crystallographic data for the four compounds in Table I; anisotropic thermal parameters; hydrogen atom coordinates (21 pages); calculated and observed structure factors (116 pages). Ordering information is given on any current masthead page.

(47) Ross, F. K.; Stucky, G. D. *J. Am. Chem. Soc.* **1970**, *92*, 4538.
(48) Gill, N. S. *J. Chem. Soc.* **1961**, 3512.